Cell Reports

Article

Histone H1 kills MRSA

Graphical abstract

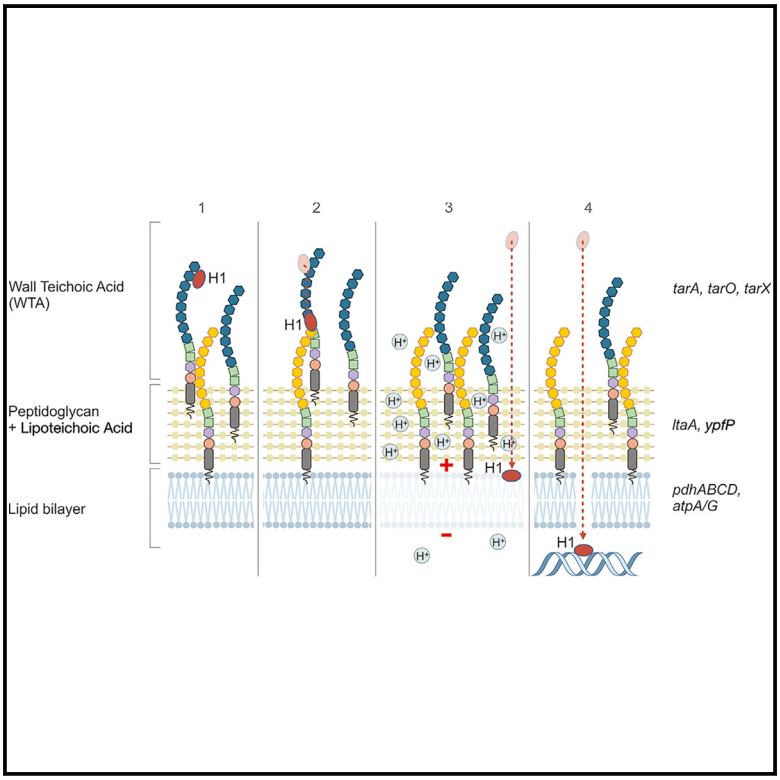

Authors

Gerben Marsman, Xuhui Zheng, Dora Čerina, ..., C.J. Harbort, Victor J. Torres, Arturo Zychlinsky

Correspondence

victor.torres@stjude.org (V.J.T.), zychlinsky@mpiib-berlin.mpg.de (A.Z.)

In brief

Marsman et al. detect histone H1 in MRSA in human abscesses and demonstrate that it kills MRSA under physiological conditions. They identify through selective evolution and a genome-wide screen that histone H1 targets wall teichoic acids and permeabilizes potentiated membranes of metabolically active and dividing cells, providing molecular insight into host-mediated clearance of MRSA.

Highlights

- Histone H1 kills MRSA under physiological conditions
- Histone H1 binds to wall teichoic acids
- Histone H1 targets the potentiated membranes of metabolically active and dividing cells

Marsman et al., 2024, Cell Reports *43*, 114969
November 26, 2024
https://doi.org/10.1016/j.celrep.2024.114969

CellPress

Cell Reports

CellPress
OPEN ACCESS

Article

Histone H1 kills MRSA

Gerben Marsman,[1,5] Xuhui Zheng,[2,5] Dora Čerina,[1] Keenan A. Lacey,[2] Menghan Liu,[2] Daniel Humme,[3] Christian Goosmann,[1] Volker Brinkmann,[1] C.J. Harbort,[1] Victor J. Torres,[2,4,6,*] and Arturo Zychlinsky[1,6,7,*]

[1]Department of Cellular Microbiology, Max Planck Institute for Infection Biology, Charitéplatz 1, 10117 Berlin, Germany
[2]Department of Microbiology, New York University Grossman School of Medicine, 430 East 29th Street, New York, NY 10016, USA
[3]Department of Dermatology, Venerology and Allergology, Charité Universitätsmedizin Berlin, corporate member of Freie Universität Berlin, Humboldt-Universität zu Berlin and Berlin Institute of Health, Berlin, Germany
[4]Department of Host-Microbe Interactions, St. Jude Children's Research Hospital, 262 Danny Thomas Place, Memphis, TN 38105, USA
[5]These authors contributed equally
[6]These authors contributed equally
[7]Lead contact
*Correspondence: victor.torres@stjude.org (V.J.T.), zychlinsky@mpiib-berlin.mpg.de (A.Z.)
https://doi.org/10.1016/j.celrep.2024.114969

SUMMARY

The antimicrobial activity of histones was discovered in the 1940s, but their mechanism of action is not fully known. Here we show that methicillin-resistant *Staphylococcus aureus* (MRSA) is susceptible to histone H1 (H1), even in the presence of divalent cations and serum. Through selective evolution and a genome-wide screen of a transposon library, as well as physiological and pharmacological experiments, we elucidated how H1 kills MRSA. We show that H1 first binds to wall teichoic acids with high affinity. Once bound, H1 requires a potentiated membrane and a metabolically active bacterium to permeabilize the membrane and enter the cell. Upon entry, H1 accumulates intracellularly, in close association with the bacterial DNA. Of note, anti-H1 antibodies inhibit neutrophil extracellular trap killing of MRSA. Moreover, H1 colocalizes with bacterial DNA in abscess samples of MRSA-infected patients, suggesting a role for H1 in combating MRSA *in vivo*.

INTRODUCTION

Histones are a family of proteins that are crucial in packaging DNA in the nucleus of eukaryotic cells. The discovery of the nucleosome in 1974 revealed histones' significance in genome organization.[1] Before this discovery, however, histones were known for their potent antimicrobial activity as antimicrobial peptides (AMPs).[2,3] Despite this, the antimicrobial function of histones received limited attention, perhaps due to the perceived unlikelihood of intranuclear histones encountering pathogens. Nonetheless, histone and histone-derived peptides were found outside the nucleus, e.g., as part of the mucosal layer of several fish and amphibians,[4–8] within lipid droplets of *Drosophila melanogaster*,[9] and on neutrophil extracellular traps (NETs),[10] which has reignited interest in understanding their antimicrobial properties.

Numerous studies describe the antimicrobial actions of the core histones H2A, H2B, H3, and H4, as well as their peptide derivatives.[4,11–15] Although the exact mechanism of their antimicrobial activity remains incompletely understood, it is suggested that histones interact with bacterial cell membranes, causing disruption of membrane integrity.[16,17] Interestingly, this activity is not limited to prokaryotic membranes; histones are also toxic to eukaryotic cells, which might contribute to inflammation.[18–22]

Histone H1 (H1), also known as the linker histone, differs from the core histones in both structure and function. While core histones possess a characteristic helix-loop-helix motif, H1's primary structure is different. H1 contains a short basic N-terminal domain, a globular domain, and an unstructured, highly positively charged C-terminal tail that consists of up to 40% of lysines (p*I* = ~11).[23,24] Unlike core histones, H1 is not part of the nucleosome core but resides on the outside at the linker DNA entry and exit sites and plays a role in higher-order chromatin organization.[25,26] As a result, H1 can dynamically shuttle between bound and unbound states within the nucleus.[27] H1 is also found in NETs released by neutrophils at inflammatory sites, and its antimicrobial potential has been recognized in several studies[4,9,28–32] but, thus far, a mechanism and a comparative perspective with other AMPs has been lacking.

The field of AMP research faces several limitations, which hinders a comprehensive interpretation of the antimicrobial properties of many of them. One of these limitations is that most *in vitro* AMP studies are conducted in saline, overlooking the potential impact of divalent cations, which can significantly reduce the antimicrobial potential of positively charged AMPs.[30,33–35] The impact of interaction between AMPs and other charged proteins in the environment is also often not taken into consideration. For example, core histones within a nucleosome may have their positive charge shielded by negatively charged DNA, lowering their antimicrobial potential.[36] Purified nucleosomes, in fact, do not exhibit antimicrobial activity against pro- or eukaryotic cells. The presence of DNA-free histones at inflammatory sites has been debated for years, and the circumstances under which

histones are released from a nucleosome, i.e., through histone modifications or DNase activity, remain unclear.[18,22,37] H1, due to its location on the nucleosome, may be more exposed than the core histone subtypes.

Staphylococcus aureus, a gram-positive spherically shaped bacterium, is a common member of the body's microbiota, often present in the upper respiratory tract and on the skin. *S. aureus*, however, is a leading cause of skin and soft-tissue infections, ranging from abscesses and boils to cellulitis. Additionally, it can cause more severe infections such as pneumonia, bloodstream infections, endocarditis, and bone and joint infections. The prevalence of antibiotic-resistant strains, particularly methicillin-resistant *S. aureus* (MRSA), is on the rise worldwide.[38,39] *S. aureus* strains are highly adaptive and can rapidly develop resistance to antibiotics or AMPs.[40]

In this study, we initially investigate the antimicrobial activity of various AMPs against MRSA in buffers reflecting physiological conditions, i.e., in tissue culture medium supplemented with serum. Most AMPs exhibited limited antimicrobial activity against MRSA. Remarkably, H1 displayed highly potent antimicrobial activity against metabolically active, dividing MRSA, under physiological conditions. Through directed evolution and transposon library screening, we elucidated that H1 sequentially targets wall teichoic acids (WTAs) and the membrane potential, and binds to MRSA DNA. Additionally, we provide evidence that supports an important role for H1 in the innate immune defense against MRSA infections. Altogether, our study demonstrates the powerful and specific antimicrobial potential of H1.

RESULTS

H1 kills MRSA under physiological conditions

AMPs are often identified by their capacity to kill microbes in solutions, e.g., saline or PBS, that do not reflect the complex environments encountered *in vivo*. Divalent cations and serum proteins present in most, if not all, biological environments, may inhibit AMPs' ability to kill.[17] We therefore tested the killing activity of 13 AMPs on MRSA, which is resistant to many antimicrobial or antibiotic challenges, in RPMI medium supplemented with 5% heat-inactivated serum. H1 killed MRSA at least two orders of magnitude more effectively than any other AMP tested (Figures 1A and 1B). Of note, H1 was not toxic to peripheral blood mononuclear cells or neutrophils at the concentrations used in this study (Figure S1A).

H1 is released from necrotic cells and through the formation of NETs at inflammatory sites.[37] An anti-H1 antibody, but not a control antibody, blocked MRSA killing by NETs, indicating that, despite the plethora of AMPs present on these structures, H1 is the main driver of *Staphylococcus* elimination (Figure 1C).

We next examined whether H1 interacts with MRSA during human infections. Analyses of abscess biopsies from MRSA-infected patients revealed that H1 interacts with *S. aureus* in abscess fluid, which contains both NETs and necrotic debris (Figure 1DI). In these biopsies, H1 localized inside the MRSA cell, as determined by immunoelectron microscopy (Figures 1DII, 1DIII, and S1B). Together, these data support the hypothesis that H1 is involved in host immunity against MRSA infections.

H1 permeabilizes MRSA and colocalizes with DNA in the cytoplasm

To study the kinetics of H1-mediated killing, we incubated MRSA with fluorescently labeled H1. Using live microscopy, we observed that H1 first binds to the cell wall and the septum of dividing MRSA in the first 15 min after initiation of the experiment (Figure 2A). Over the 2-h course of the experiment, H1 progressively enters MRSA (Figures 2A and 2D). As measured by the fluorescent probe DiOC2(3), H1 reduced the membrane potential within 15 min, indicating that H1 binding disrupts the barrier function of the cell membrane for ions (Figure 2B). Meanwhile, we detected a rapid H1-mediated leakage of ATP from MRSA, plateauing within 30 min post H1 challenge (Figure 2C). Notably, this effect was dose dependent. Furthermore, using immune electron microscopy, we found that H1 (large gold particles) colocalized with bacterial DNA (small gold particles) (Figures 2E and 2F).

We next examined the effect of H1 internalization on MRSA. We incubated MRSA with fluorescent H1 and after 30 min sorted the cells into "dim" (surface-bound H1) vs. "bright" (internalized H1) populations. We plated equal numbers of bacteria but recovered 10-fold more colony-forming units (CFU) of MRSA with surface-bound H1 than with internalized H1 (Figure 2G), indicating that internalized H1 is associated with more efficient killing of MRSA. We also measured MRSA metabolic activity using the Alamar blue dye, which reports on the reductive intracellular environment of living cells. H1, but not other histones, block the metabolic activity of MRSA in unsupplemented RPMI medium (Figure 2H) but not in saline (Figure S2A). These data suggest that H1 kills MRSA through entering the cytoplasm and inhibiting metabolic activity in addition to binding to the cell surface and permeabilizing the cell membrane.

To identify whether a specific domain in H1 is responsible for the toxicity to MRSA, we compared the killing activity of the N-terminal tail, the globular domain, and the unstructured, highly positively charged C-terminal tail. Interestingly, only the C-terminal tail of H1 was toxic to MRSA but never reached the toxicity conferred by the complete protein (Figure 2I). Mixing the three individual domains in equal molar ratios did not increase the antimicrobial effect. Furthermore, the toxicity of the C-terminal tail was not determined by its primary structure, as a scrambled version was equally as toxic as the wild-type (WT) C-terminal tail.

The membrane potential and the proton gradient mediate MRSA sensitivity to H1

Given the highly positive charge of H1 and the relative negative charge of the intracellular environment of MRSA, we proposed that the proton-motive force (PMF) may be involved in modulating the sensitivity of MRSA. One component of the PMF is the membrane potential, which is impacted by H1 (Figure 2B). We lowered the membrane potential of MRSA with the potassium ionophore valinomycin (Figure 3A) without affecting MRSA viability (Figure 3B). As a positive control for the modulation of the membrane potential, we used the potent protonophore carbonyl cyanide-chlorophenyl hydrazone (CCCP). Interestingly, valinomycin attenuated H1 (5 μM) antimicrobial activity but not that of 20 μM LL37 (Figure 3B), which is toxic

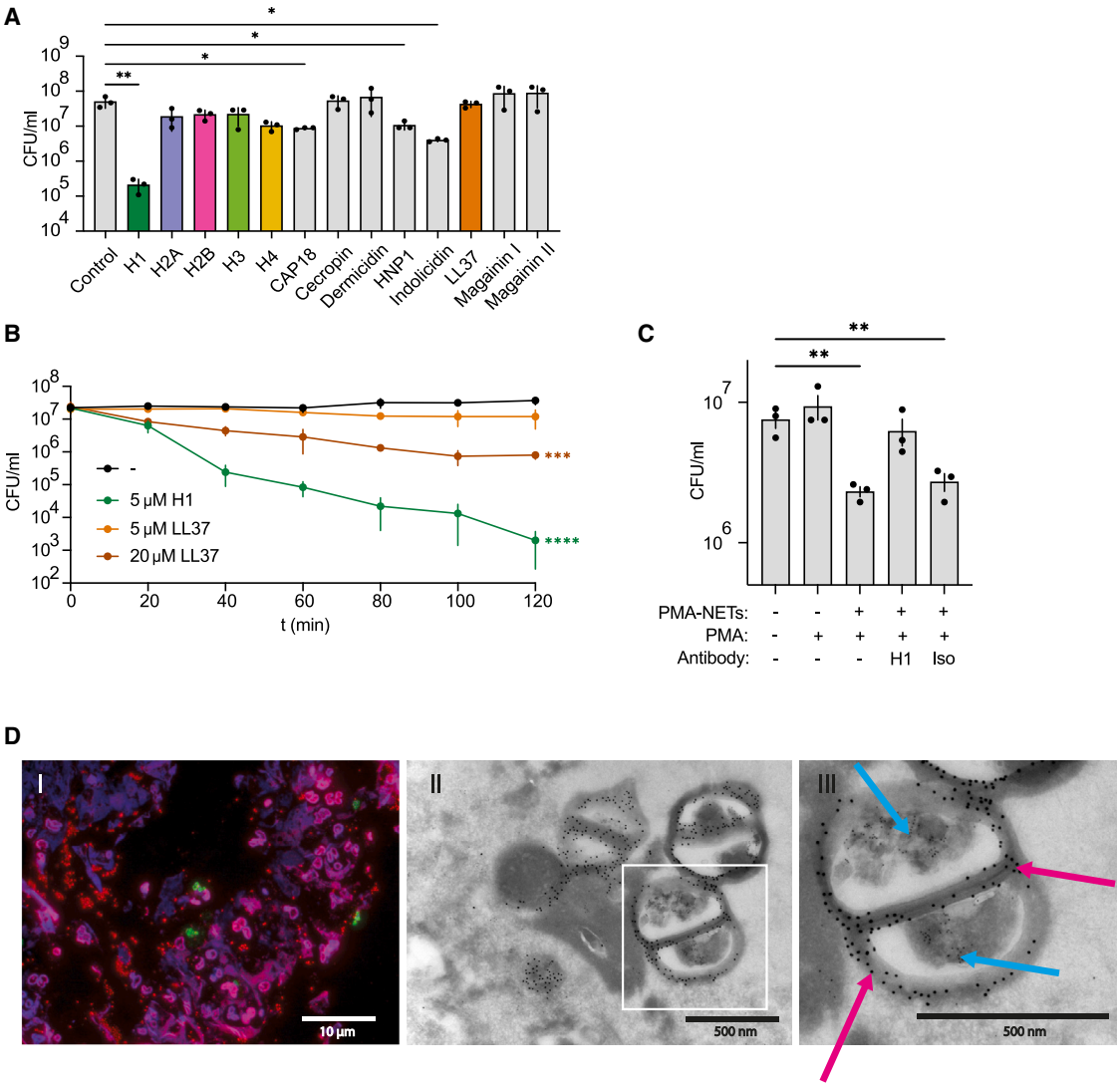

Figure 1. Histone H1 kills MRSA and is found in MRSA-containing abscesses

(A) MRSA was incubated with 5 μM histones H1, H2A, H2B, H3, and H4, CAP18, cecropin, dermcidin, HNP1, indolicidin, LL37, magainin I, or magainin II for 2 h in RPMI medium supplemented with 5% heat-inactivated human serum and plated. The figure shows colony-forming units (CFU) after overnight incubation. Data are from three independent experiments presented as the mean ± SEM. Statistical significance was determined on log-transformed data by one-way ANOVA with Dunnett's multiple comparison (*$p \leq 0.05$; **$p \leq 0.01$).

(B) MRSA was incubated with histone H1 (H1) or LL37 at the indicated concentrations and plated at 20-min intervals. The plot shows CFU after overnight incubation. Data are from three independent experiments presented as the mean ± SEM. Statistical significance was determined on log-transformed data of the 120-min time point by one-way ANOVA with Dunnett's multiple comparison (***$p \leq 0.001$; ****$p \leq 0.0001$).

(C) MRSA was incubated for 1 h on phorbol 12-myristate 13-acetate (PMA)-induced NETs pre-incubated with or without an anti-H1 antibody or an isotype control and plated. The plot shows CFU after overnight incubation. Data are from three independent experiments presented as the mean ± SEM. Statistical significance was determined on log-transformed data by one-way ANOVA with Dunnett's multiple comparison (**$p \leq 0.01$).

(D) (I) An abscess biopsy from an MRSA-infected patient probed for DNA (blue), H1 (red), and *S. aureus* protein A (green) and visualized by confocal microscopy. (II and III) Transmission electron microscopy of the same sample as in (I) probed for H1 (12 nm gold, blue arrows) and protein A (18 nm gold, pink arrows). The white box in (II) indicates the area enlarged in (III).

to MRSA (Figure 1B). Conversely, the ATP-synthase inhibitor oligomycin, as expected,[41–43] increased the membrane potential of MRSA (Figure 3A), which potentiated the antimicrobial activity of H1 but not of LL37 (Figure 3B). This suggests that the membrane potential plays a deterministic role in the sensitivity of MRSA to H1. We also addressed the involvement of the proton gradient, the second component of the PMF, by incubating MRSA with the proton ionophore nigericin. Nigericin is an H^+/K^+ antiporter, allowing for an electroneutral exchange of protons, dissipating the proton gradient while preserving the membrane potential. Nigericin completely protected the bacteria from H1 but exacerbated the antimicrobial activity of LL37 (Figure 3B). Furthermore,

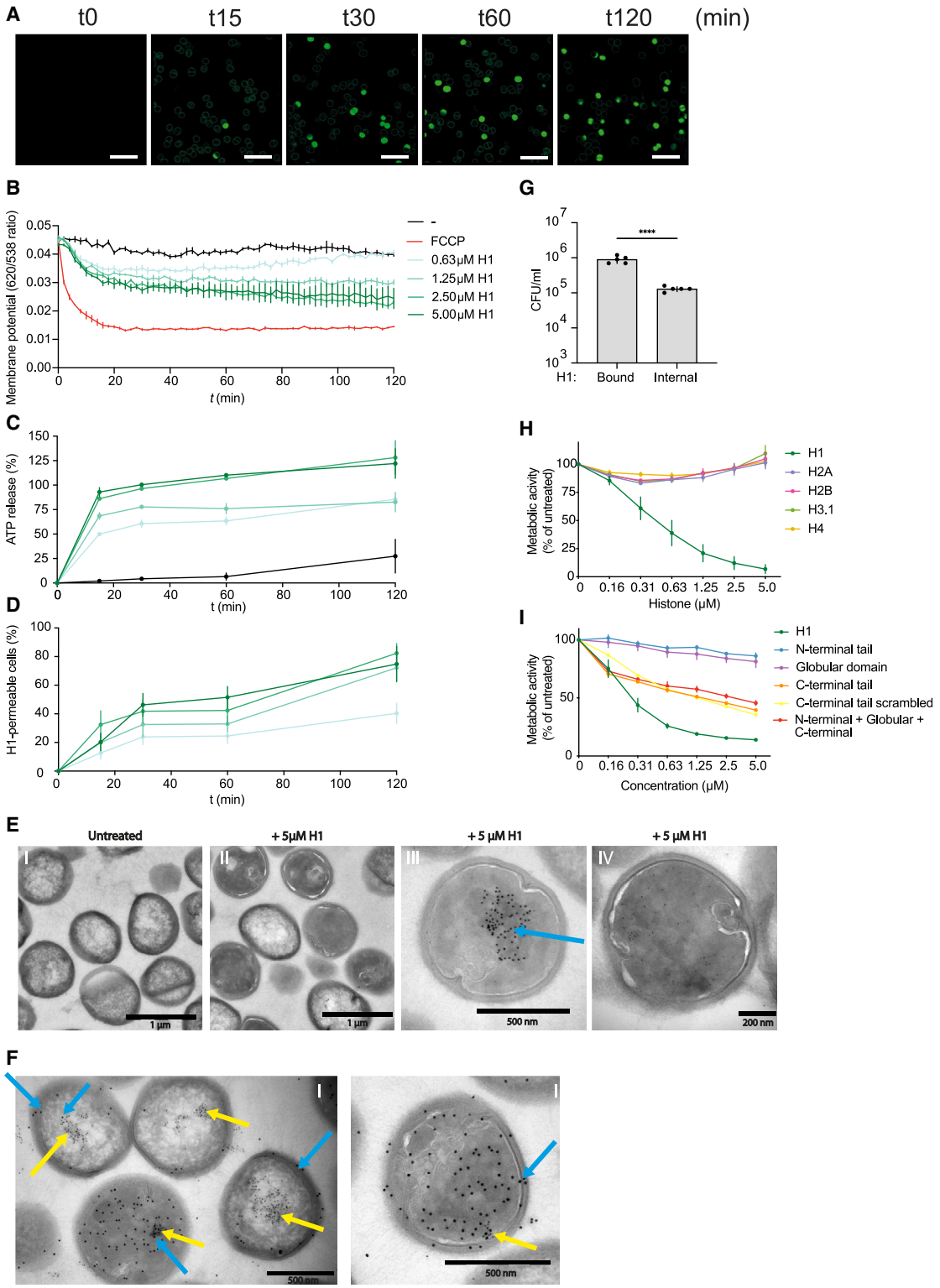

Figure 2. Histone H1 permeabilizes the membrane of MRSA and binds intracellularly to double-stranded DNA

(A and D) MRSA permeability after incubation with 1 μM Alexa Fluor 647-labeled histone H1 (H1) at the indicated time points by confocal microscopy (A) and flow cytometry (D). Scale bars, 5 μm.

(legend continued on next page)

H1 killed MRSA more efficiently at higher pH (low extracellular proton concentration, weak proton gradient) compared to low pH (high extracellular proton concentration, strong proton gradient) (Figure 3C). Together, these results suggest that both the membrane potential and the proton gradient modulate the sensitivity of MRSA to H1.

H1 targets metabolically active cells

Since the PMF is linked to energy metabolism and division, we tested whether metabolic activity is a requirement for H1 killing. We incubated MRSA in unsupplemented RPMI medium in the absence of glucose with 5 μM H1 and observed that MRSA was protected from H1 killing (Figure 4A). Furthermore, MRSA was equally susceptible to H1 in the presence of other carbon sources as in the presence of glucose (Figure S2B), indicating the requirement of an energy source for H1 to kill MRSA. Interestingly, initial H1 binding to MRSA, as measured by fluorescence-activated cell sorting (FACS), was not affected in the absence of glucose (Figure 4B).

The lack of a carbon source abrogates growth of MRSA, and we found that modulation of PMF components slows but does not block proliferation (Figure S2C). Given that metabolic activity and replication are linked, we tested whether cell division is a requirement for H1 killing. Indeed, γ-ray-irradiated MRSA, whereby the genetic insult prevents division but has no immediate effect on metabolic activity, was considerably resistant to H1 (Figure 4C). There was no synergistic protection in lowering the membrane potential with valinomycin in irradiated MRSA, and treatment with oligomycin turned out to be toxic. Furthermore, bacteriostatic antibiotics chloramphenicol and rifampicin also prevented H1 killing (Figure 4D). Together, these results show that H1 sensitivity requires metabolically active and dividing MRSA.

Directed evolution of MRSA reveals pathways involved in H1 sensitivity

To unearth potential mechanisms underlying H1 killing of MRSA, we evolved MRSA strains to become resistant to H1. MRSA was cultured in unsupplemented RPMI medium in the presence of 1 μM H1 for 24 h, after which the culture was diluted 1:100 on a daily basis into fresh RPMI medium with the same histone concentration (Figure 5A). By using this concentration of histone we aimed to have stringent selection conditions, but not kill all bacteria in the culture. We quantified resistance of the culture to 5 μM H1 daily until we obtained over 80% resistance. Resistance appeared between 14 and 21 days of serial incubation with H1 in three independent experiments (Figures 5B and S3A), and we called the three resulting evolved cultures Evo1, Evo2, and Evo3, with the corresponding controls Ctrl1, Ctrl2, and Ctrl3. These controls, which did not become resistant to H1, were generated by daily dilution in the absence of H1. Interestingly, although the cultures were selected in 1 μM H1, the evolved cultures were resistant to significantly higher concentrations of the histone (Figure 5B). The three evolved cultures were resistant to H1 penetration (Figure 5C) and the H1-induced release of ATP (Figure 5D). Importantly, the evolved cultures acquired resistance specifically to H1, since their sensitivity to LL37 (Figure 5E) or to vancomycin (Figure 5F) were not affected. These findings suggest that H1 kills MRSA through a mechanism distinct from that of LL37 and vancomycin.

We sequenced up to 20 single colonies from each evolved culture and identified three unique genetic signatures linked to resistance (Figures 5G and S3D; Table S1). Compared to the control cultures, all Evo1 strains contained a missense mutation in the *atpG* gene with all except one having independent frameshift/missense/nonsense mutations in the *tcyABC* operon, Evo2 strains have missense mutations in the *pdhABCD* operon and the *vraG* gene, and Evo3 strains have a frameshift mutation in the *tarA* gene and different missense mutations in the *codY* gene. We observed significantly reduced expression of *atpG* and *tcyABC* genes in Evo1 mutants and increased *pdhC* but decreased *vraG* expression in Evo2 mutants (Figures S3E and S3F). These findings indicate that the mutations generated during the evolution experiment affected the expression of targeted (mutant) genes. We considered the mutations in *atpG*, *pdh*, and *tarA* as founder mutations, since they were identified in all the clones of each Evo culture (Figure 5G). We generated knockouts of the genes mentioned above in the WT strain and observed moderate (Δ*pdhA*, Δ*pdhB*, Δ*pdhC*, and Δ*pdhD* mutants) to complete resistance (Δ*tarA* and Δ*tarO* mutants) to H1 (Figure 5H). Interestingly, Evo1 and Evo2 had a lower membrane potential than their control culture or WT MRSA (Figure 5I). This suggests that the mutations in *atpG*, *tcyABC*, *pdh*, and *vraG* drive resistance to H1 by lowering the membrane potential. No changes

(B) Time course of the membrane potential of MRSA pre-incubated with the membrane potential dye DiOC2(3) and challenged with H1 at the indicated concentrations or with the proton uncoupler carbonyl cyanide-4(trifluoromethoxy) chlorophenyl hydrazone (FCCP). Data are from three independent experiments presented as the mean ± SEM.

(C) Quantification of ATP levels in the supernatant of MRSA cultures 15, 30, 60, and 120 min after incubation with H1 at the concentrations indicated in (B). Data are from three independent experiments presented as the mean ± SEM.

(D) Quantification of the percentage of MRSA permeabilized by H1 as determined by flow cytometry after incubation with AF488-labeled H1 at the concentrations indicated in (B). Data are from three independent experiments presented as the mean ± SEM.

(E) Transmission electron microscopy (TEM) of untreated MRSA (panel I) or MRSA incubated with biotinylated H1 for 60 min and probed for H1 using an anti-H1 antibody (12 nm gold; panel II) or anti-biotin (5 nm gold; panels III and IV). Scale bar calibrations are indicated.

(F) TEM of MRSA incubated with biotinylated H1 for 60 min and probed with anti-biotin (15 nm gold, blue arrows) or an anti-double-stranded-DNA antibody (12 nm gold, yellow arrows). Scale bar calibration is indicated.

(G) Quantification of survival of MRSA incubated for 30 min with 1 μM H1, sorted for bacteria with surface-bound or internal H1, concentrations adjusted to 10^6/mL, and plated. CFU were counted after an overnight incubation. Data are from five independent experiments presented as the mean ± SEM. Statistical significance was determined by a two-tailed paired t test (****$p \leq 0.0001$).

(H and I) Quantification of the conversion of the Alamar blue dye as a proxy for metabolic activity of MRSA incubated with the indicated histones (H) or synthetic fragments of H1.2 (I) for 60 min. Data are from three independent experiments presented as the mean ± SEM.

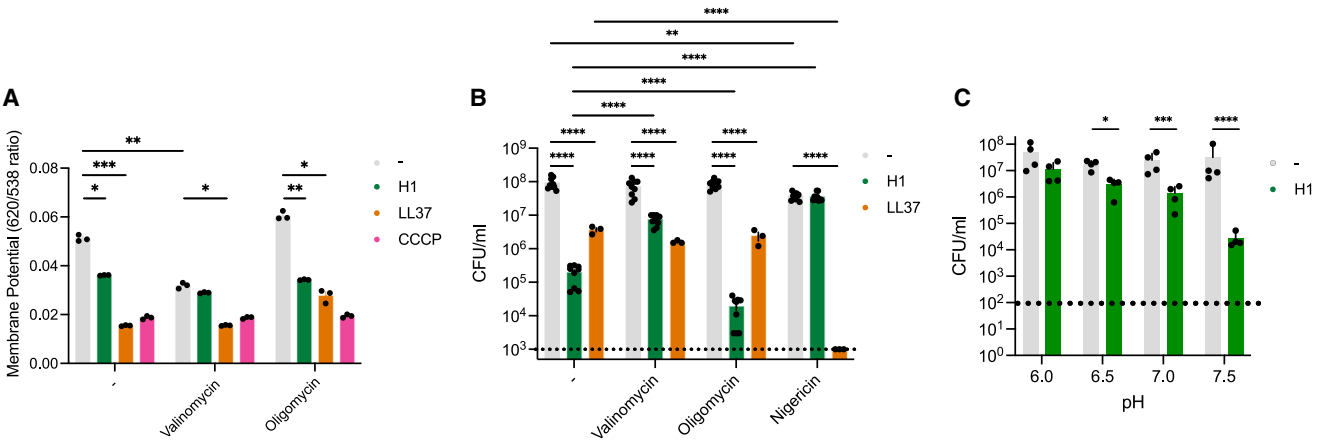

Figure 3. The proton-motive force modulates sensitivity to histone H1

(A and B) Quantification of the MRSA membrane potential using the fluorescent dye DiOC2(3). The membrane potential was modulated using 5 μM valinomycin or 8 μg/mL oligomycin prior to incubation with 5 μM histone H1 (H1) or 20 μM LL37. Quantification of the membrane potential 60 min post treatment with H1 or LL37 (A) as well as the CFU (B). Data are from 3–8 independent experiments presented as the mean ± SEM. Statistical significance was determined on untransformed (A) or log-transformed (B) data by two-way ANOVA with Tukey's multiple comparison (*$p \leq 0.05$; **$p \leq 0.01$; ***$p \leq 0.001$; ****$p \leq 0.001$).

(C) Viability, expressed as CFU, of MRSA incubated with 5 μM H1 in RPMI medium at pH 6.0, pH 6.5, pH 7.0, or pH 7.5 for 120 min. Data are from three independent experiments presented as the mean ± SEM. Statistical significance was determined on log-transformed data by two-way ANOVA with Tukey's multiple comparison (*$p \leq 0.05$; ***$p \leq 0.001$; ****$p \leq 0.001$).

in division rates were observed (Figures S3B and S3C). Notably, raising the membrane potential of Evo1 and Evo2 through oligomycin treatment was lethal, suggesting that the genetic changes resulting in a decreased membrane potential had increased H1 resistance but at a cost of metabolic flexibility.

Identification of genes involved in H1 sensitivity through transposon mutant library screening

Independently, we also screened the Nebraska Transposon Mutant Library containing 1,952 individual transposon insertion mutants in nonessential genes[44] for increased sensitivity or resistance against 1 μM H1, 20 μM LL37, 1 μg/mL vancomycin, and 1 μg/mL daptomycin, and plotted the 40 mutants with the highest resistance or sensitivity to H1 (Figure 6A and Table S2). As expected, we identified genes required for the expulsion of positively charged AMPs such as *graRS* and *vraFG* (red cluster). Importantly, H1 resistance was altered in mutants of protein complexes also identified in the selective evolution approach including *atpA*, *pdhB*, and *lpdA* (*pdhD*). Of note, mutants of *tarA* or *tarO* are not present in the library. Results from the Alamar blue metabolic assay correlated well with growth measured by OD_{600} in these 80 mutants (Figure 6B). There was also a strong

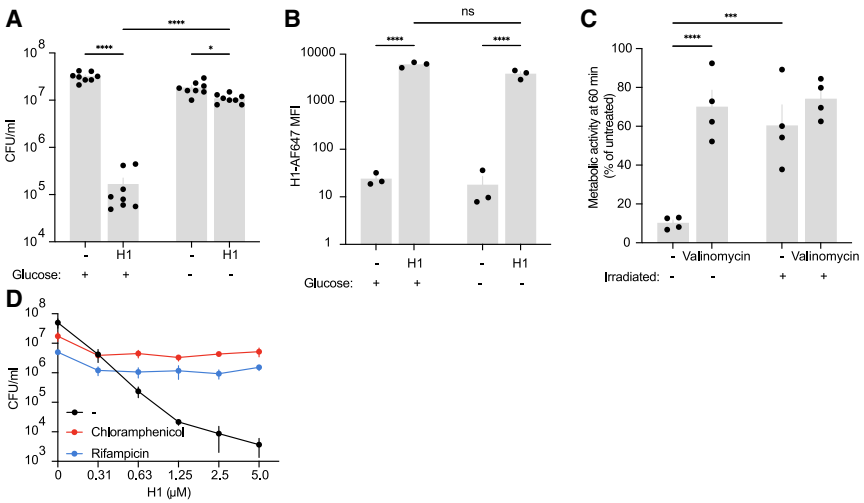

Figure 4. MRSA requires metabolic activity and division to be sensitive to histone H1

(A) CFU of MRSA incubated with 5 μM histone H1 (H1) for 120 min in the absence or presence of glucose. Data are from eight independent experiments presented as the mean ± SEM. Statistical significance was determined by two-way ANOVA (*$p \leq 0.05$; ****$p \leq 0.0001$).

(B) Flow-cytometry quantification of H1-AF647 (1 μM) binding to MRSA after 15-min incubation in the absence or presence of glucose. Data are from three independent experiments presented as the mean ± SEM. Statistical significance was determined by two-way ANOVA (****$p \leq 0.0001$; ns, not significant).

(C) Metabolic activity, measured through conversion of Alamar blue, of MRSA irradiated overnight with ~0.9 kGy to block division. Irradiated bacteria were incubated with or without 5 μM valinomycin prior to incubation with 5 μM H1 for 60 min. Data are normalized to the indicated conditions in the absence of H1. Data are from four independent experiments presented as the mean ± SEM. Statistical significance was determined by two-way ANOVA (***$p \leq 0.001$; ****$p \leq 0.0001$).

(D) Metabolic activity, measured through conversion of Alamar blue, of MRSA incubated with 37 μg/mL chloramphenicol or 10 μg/mL rifampicin to prevent division, prior to incubation with H1 for 60 min. Data are from three independent experiments presented as the mean ± SEM.

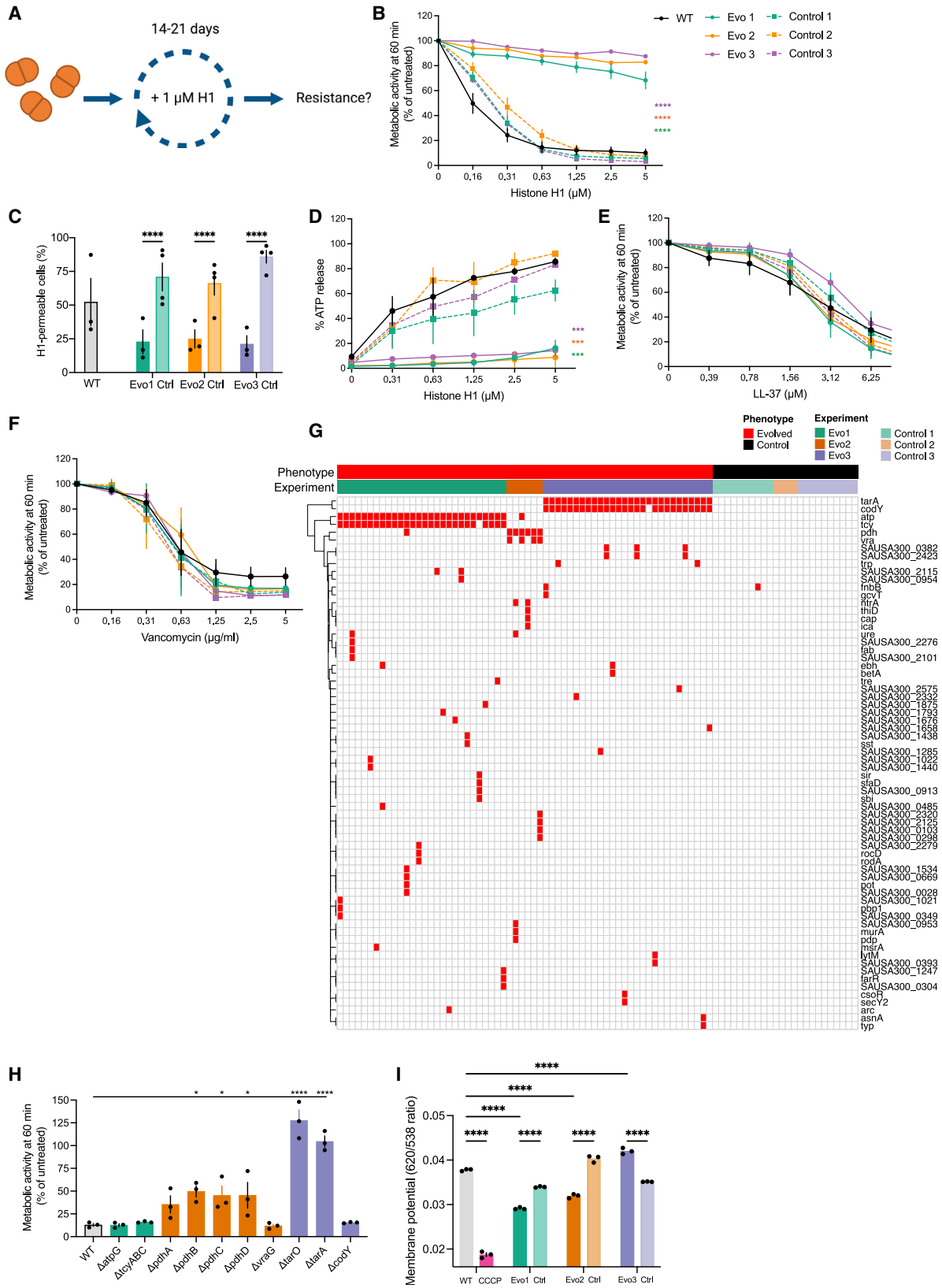

(legend on next page)

correlation between sensitivity to H1 and baseline metabolic activity within the group of 80 mutants (Figure 6C), again suggesting a link between growth/division and H1 killing. The sensitivity to H1 and LL37 correlated, although we did not observe mutants with increased resistance to LL37 (Figures 6D and S4A). Notably, mutants with increased susceptibility to H1 and LL37 showed a tendency to positively correlate ($x < 0$, trend line in red), while mutants with increased resistance to H1 ($x > 0$, trend line in green) did not show increased resistance to LL37. This suggests that susceptibility mechanisms are shared between LL37 and H1, while resistance mechanisms are specific. Interestingly, the sensitivity to H1 and the positively charged antibiotic daptomycin correlated (Figure S4B). Based on this screen, we selectively transduced the mutations of *tarX*, *ychF*, *fmtA*, and *trkA* into a WT strain and performed complementation studies. These results corroborated that these gene products were responsible for the sensitivity to H1 (Figures 6E–6H and S4C). Of note, we did not investigate the mutants in cluster 2, as these mutants were severely affected in metabolic activity and growth, indicating that growth is a factor that drives H1 sensitivity. Due to the modulatory effect of multiple genes on the antimicrobial potential of H1 in MRSA, we asked whether the sensitivity to H1 is conserved between different *S. aureus* clinical isolates and clonal complexes (CCs). Indeed, we found a wide variation in sensitivity, with the highest level of resistance found in *S. aureus* CC45 isolates (Figures S4D and S4E; Table S3).

H1 targets gram-positive bacteria by binding to wall teichoic acid

We identified, both in the directed evolution approach (*tarA*, *tarO*) and in the transposon library screen (*tarX*), that killing by H1 seems to require WTA synthesis. To extend these findings, we purified WTAs from WT MRSA and from the three evolved cultures and their controls. Indeed, in Evo3, the *tarA* mutation inactivates the gene completely and renders MRSA deficient for WTAs (Figure 7A). As a control, we incubated WT MRSA with tunicamycin, a specific inhibitor of TarO, to inhibit WTA synthesis. H1 bound poorly to either Evo3 or tunicamycin-treated WT MRSA (Figure 7B) and did not affect the metabolic activity of either strain (Figure 7C). Interestingly, Evo3 and tunicamycin-treated WT MRSA were susceptible to LL37 or vancomycin (Figures 7D and 7E). Purified WTAs protected WT MRSA from H1 killing in a concentration-dependent manner (Figure 7F), suggesting that WTAs could be the H1 receptor. Microscale thermoelectrophoresis revealed that H1 interacts directly with WTAs with a K_D of ~300 nM. Finally, complementation of the *ΔtarA* and *ΔtarO* strains reconstituted the synthesis of WTAs and restored the sensitivity to H1 (Figures 7A and 7H).

WTAs are a major component of the cell wall of gram-positive bacteria. As such, we tested other clinically relevant gram-positive pathogens for sensitivity to H1. We confirm sensitivity of both group A and group B *Streptococci* to H1 (Figures S5A and S5B). In contrast, the gram-negative bacterium *Escherichia coli* was resistant to H1 (Figure S5C). In addition to the WTAs tethered to the peptidoglycan layer, *S. aureus* produces lipoteichoic acid (LTAs), which are similar in structure compared to WTAs but are tethered to the lipid bilayer. Genes required to synthesize LTAs are, in contrast to WTA-synthesis genes, essential for MRSA. However, we found that *ltaA* and *ypfP* mutants, which are known to generate longer polymers of LTA, displayed increased susceptibility to killing by H1 (Figure 7I). Collectively, these data indicate that teichoic acids are the primary target for H1.

DISCUSSION

Our evolution experiments generated a strain deficient in WTA synthesis, which led us to investigate the role of WTAs in H1-mediated killing. WTAs are anionic phosphate-rich glycopolymers tethered to the peptidoglycan layer of gram-positive bacteria and are part of the meshwork that make up their cell wall.[45–47] LTAs are similar in structure to WTAs but are tethered to the plasma membrane through their glycolipid end. WTAs carry modifications that contribute to shielding the negative charge of the polyribitol-phosphate backbone.[48,49] WTAs and LTAs, i.e., teichoic acids, are intimately involved in many aspects of

Figure 5. Generation of resistance to histone H1 through *in vitro*-directed evolution

(A) Scheme of the experiment to generate histone H1 (H1)-resistant MRSA by directed *in vitro* evolution. MRSA cultures were passaged 1:100 every 24 h for 14–22 days with or without 1 μM H1. We tested viability after incubation with 5 μM H1 daily until >80% viability was obtained.

(B) Quantification of the endpoint resistance to H1 in three independent evolution experiments by Alamar blue conversion. Data are from three independent experiments presented as the mean ± SEM. Statistical significance was determined by one-way ANOVA of the 5 μM H1 concentration with Dunnett's multiple comparison (****$p \leq 0.0001$). Asterisks indicate a comparison with the wild-type (WT) strain.

(C) Quantification of the permeabilization of MRSA evolved cultures by flow cytometry using 1 μM H1-AF647. Data are from three independent experiments presented as the mean ± SEM. Statistical significance was determined by two-way ANOVA with Tukey's multiple comparison (****$p \leq 0.0001$).

(D) Quantification of ATP release into the supernatant after 60 min of incubation with the indicated H1 concentrations. Data are from three independent experiments presented as the mean ± SEM. Statistical significance was determined by one-way ANOVA of the 5 μM H1 concentration with Dunnett's multiple comparison (***$p \leq 0.001$). Asterisks indicate a comparison with the WT strain.

(E and F) Quantification of metabolic activity by Alamar blue conversion of the evolved cultures after 60-min incubation with 20 μM LL37 (E) or 1 μg/mL vancomycin (F). Data are from three independent experiments presented as the mean ± SEM.

(G) Sequencing results of individual colonies picked from the three evolution experiments. Each column represents one colony, and each row represents a genetic function unit (a gene or an operon) that has mutations in the Evo strain but not the respective control strain. The red bar indicates H1-resistant colonies and the black bar colonies picked from the control cultures. Green indicates colonies picked from Evo1, orange from Evo2, and purple from Evo3.

(H) Quantification of metabolic activity by Alamar blue conversion of knockouts after 60-min incubation with 5 μM H1. Data are from three independent experiments presented as the mean ± SEM. Statistical significance was determined by one-way ANOVA with Dunnett's multiple comparison (*$p \leq 0.05$; ****$p \leq 0.0001$).

(I) Quantification of the membrane potential of the evolved H1-resistant clones determined through DiOC2(3) staining. Data are from three independent experiments presented as the mean ± SEM. Statistical significance was determined by two-way ANOVA with Tukey's multiple comparison (****$p \leq 0.0001$).

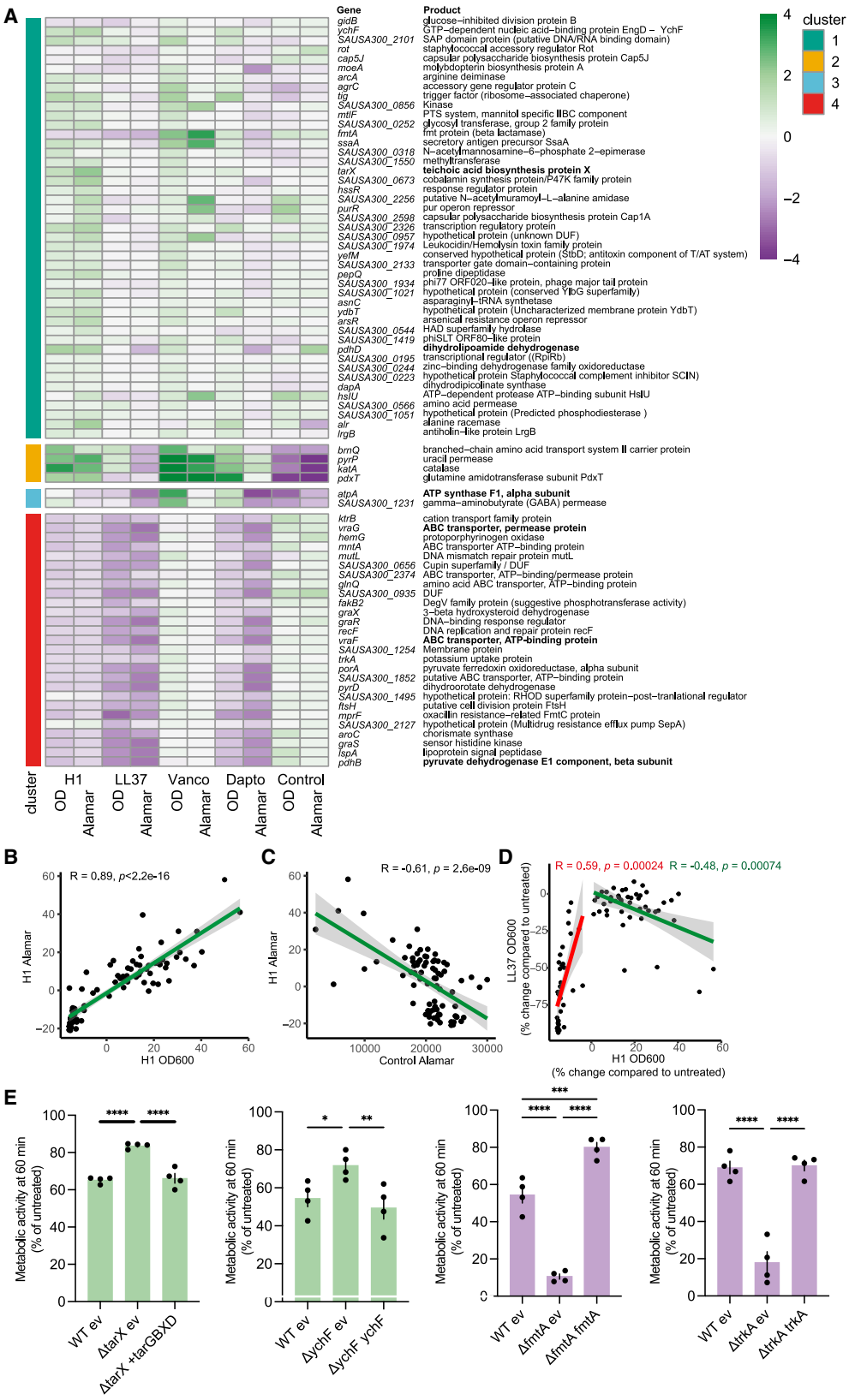

(legend on next page)

cell physiology, including division, autolysin activity, and antibiotic resistance.[50–53] Moreover, WTA-deficient *S. aureus* strains display reduced virulence *in vivo*, probably because WTAs play an important role in adhering to the tissues of the invaded organism and in establishing an infectious niche.[54]

The culture Evo3 is a mutant of *tarA*, which encodes an essential enzyme for WTA synthesis (Figure 5G).[47] Furthermore, while the *tarA* mutant is not present in the transposon library, the transposon mutant of *tarX*, which is part of the WTA-synthesis operon, showed increased resistance to H1 but not to LL37, (Figure 6A). Correspondingly, mutants of *vraF*/*vraG*, *graR*/*graS*, and *fmtA*, genes that make up the sensing system for cationic AMP and regulate D-alanylation of teichoic acids, were found to be hypersensitive to H1. The importance of WTAs in H1-mediated killing is further supported by the susceptibility of other gram-positive pathogens but not of *E. coli*, a representative of gram-negative bacteria, to H1 (Figures S5A–S5C). Based on these data, we propose that H1 initially binds to WTAs exposed on the peptidoglycan layer and then diffuses through the meshwork using both WTAs and LTAs to reach the cell membrane.

After binding to teichoic acids, H1 damages the plasma membrane. We found that the PMF, which sustains a relative negative electrochemical charge, plays a key role in modulating sensitivity to H1. We hypothesize that this negative charge may facilitate H1 to move through the mesh of WTAs and LTAs to the cell membrane. The PMF is composed of the membrane potential and the proton gradient (ΔpH). Dissipation of the membrane potential through valinomycin treatment rendered MRSA resistant to H1, while an increase through oligomycin treatment rendered it more sensitive (Figures 3A and 3B). This was not observed for LL37, also a highly cationic molecule. Oligomycin is an inhibitor of ATP synthase. Whereas ATP synthase in most organisms uses the energy stored in ΔpH to generate ATP with protons shuttling back into the cell, the ATP synthase in *S. aureus* acts in reverse and pumps out protons at the cost of ATP.[55] Inhibition of ATP synthase therefore prevents *S. aureus* from maintaining the ΔpH. *S. aureus* has been described to sustain a relatively constant PMF when either the membrane potential or the ΔpH are modulated by external factors.[56,57] As a response to lowering of the ΔpH by oligomycin, *S. aureus* increases the membrane potential, an effect we also observed (Figure 3A), rendering *S. aureus* more sensitive to H1. To dissect the contributions of the membrane potential and the ΔpH to the PMF, we also incubated MRSA with nigericin. Nigericin is a potassium-proton antiporter, facilitating an electroneutral exchange of potassium and protons, resulting in the dissipation of the proton gradient while keeping the membrane potential intact. Indeed, incubation with nigericin rendered MRSA resistant to H1. Altogether, our results suggest that both the proton gradient and the membrane potential modulate the sensitivity to H1. Additionally, the PMF is essential in (cell wall) homeostasis, and its disruption could affect WTA/LTA synthesis.

Evo1 and Evo2 had mutations in *atpG* and *pdhB*/*pdhC* (Figure 5), and transposon screen mutants of *atpA*, *pdhB*, and *pdhD* displayed altered sensitivity to H1. *atpA* and *atpG* encode for subunits of the ATP-synthase complex, while *pdhB*, *pdhC*, and *pdhD* encode for subunits of the pyruvate dehydrogenase complex (PDHC). Both the ATP-synthase complex and the PDHC have central roles in *S. aureus* energy metabolism.[58] We identified that the membrane potential of Evo1 and Evo2, but not the Ctrl1 and Ctrl2 cultures, was decreased compared to WT (Figure 5I). In addition to the resistance observed in MRSA whereby the membrane potential was pharmacologically decreased using valinomycin (Figure 3B), these results further support the idea that the membrane potential is an important determinant for H1 sensitivity. We tried to pharmacologically increase the membrane potential in Evo1 and Evo2 through oligomycin treatment, but this turned out to be lethal for these cultures, suggesting that the resistance to H1 was generated at the cost of inflexibility to changes in the PMF.

Generating the PMF requires energy, and we demonstrated that a carbon energy source is crucial for making MRSA sensitive to H1 (Figure 4). Although binding of H1 to MRSA does not need a carbon source, maintaining metabolic activity and cell division does. To investigate cell division as a factor in H1 susceptibility, we found that both γ-irradiation and bacteriostatic antibiotics,

Figure 6. Transposon library screen identifies genes involved in modulating sensitivity to histone H1

(A) Quantification of viability of 1,952 USA300-JE2 transposon mutants incubated with 1 μM histone H1 (H1), 50 μg/mL LL37, 1 μg/mL vancomycin, or 1 μg/mL daptomycin for 60 min through either Alamar blue conversion (Alamar) or growth (OD_{600}) at 6 h. The percent change in the reduction of OD and Alamar blue conversion upon treatment with antimicrobials compared to wild type was calculated. The top 40 mutants with either the highest sensitivity or the highest resistance to H1 are shown (purple: more sensitive; green: more resistant). Percent changes in viability were scaled by standard deviation without mean-centering to preserve 0 as the wild-type value. Mutants were grouped into clusters, indicated by the colored bars on the left, in an unsupervised manner by *k*-means clustering based on OD and Alamar percent changes for all tested antimicrobials. The first (turquoise) cluster tends to contain mutants with an unchanged or increased resistance to H1. The second (orange) cluster tends to contain mutants with an increased resistance to H1 and vancomycin and a decreased metabolic activity and division rate. The third (blue) cluster tends to contain mutants with a decreased metabolic activity and division rate and decreased resistance to LL37. The fourth (red) cluster tends to contain mutants with increased sensitivity to H1, LL37, and daptomycin. Gene names to which the mutation can be mapped are provided if known, and the corresponding protein products are indicated. Operons that have been identified to carry mutation(s) in H1-resistant clones in the directed evolution experiment are indicated in bold.

(B and C) Percent change of metabolic activity after incubation with 1 μM H1 of the mutants in (A) as determined by Alamar blue, plotted as a function of the change observed in OD_{600} (B) or as a function of the metabolic activity of untreated bacteria (C). A positive value indicates that the strain is more resistant to H1. Statistical significance was determined by Pearson correlation test where the coefficient of correlation (*R*) and probability (*p*) are indicated.

(D) Percent change in OD_{600} as a result of LL37 incubation plotted as a function of the change in OD_{600} due to H1 incubation. Statistical significance was determined by Pearson correlation test where the coefficient of correlation (*R*) and probability (*p*) are indicated.

(E) Verification of selected transposon mutants. The transposon insertions were transduced to a clean background. The mutants were complemented with an empty vector (ev) or with a vector expressing these genes with their native promoter elsewhere in the chromosome. Colors refer to the direction of change in H1 sensitivity observed in (A). Data are from four independent experiments presented as the mean ± SEM. Statistical significance was determined by one-way ANOVA with Dunnett's multiple comparison (*$p \leq 0.05$; **$p \leq 0.01$; ***$p \leq 0.001$; ****$p \leq 0.0001$).

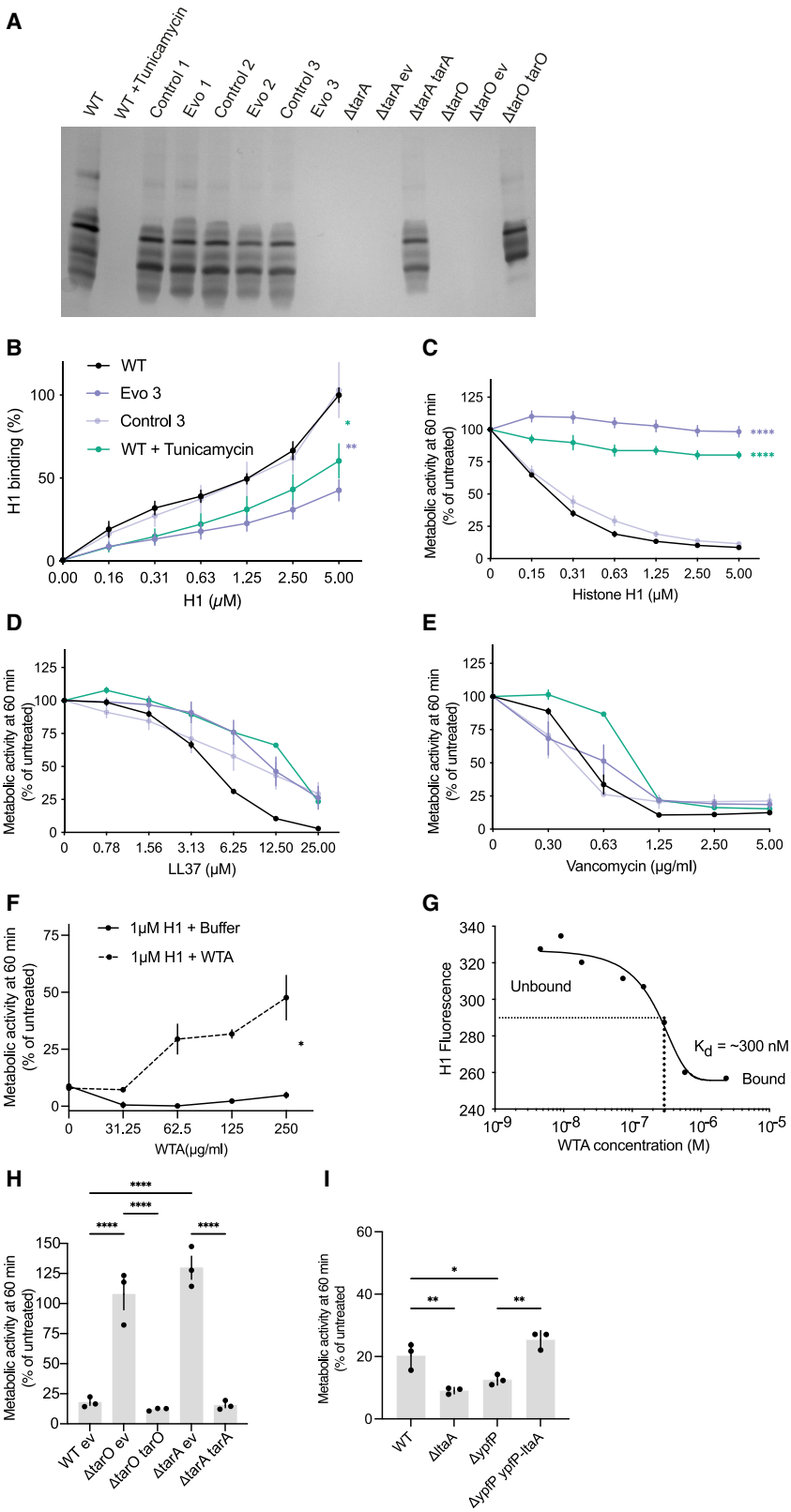

Figure 7. Wall teichoic acids are the first target of histone H1

(A) Silver-stained gel of wall teichoic acids that were purified from wild-type (WT) MRSA, the evolved histone H1 (H1)-resistant cultures, and *ΔtarA* and *ΔtarO* mutants. WT MRSA incubated with the WTA-synthesis inhibitor tunicamycin serves as negative control.

(B) Quantification by flow cytometry of H1-AF488 binding to Evo3 or to tunicamycin-treated WT. Data are from four independent experiments presented as the mean ± SEM. Statistical significance was determined by one-way ANOVA of the 5 μM H1 concentration data with Dunnett's multiple comparison (*$p \leq 0.05$; **$p \leq 0.01$).

(C–E) Quantification of metabolic activity, determined by Alamar blue conversion, of Evo3, Ctrl3, WT, or WT incubated with tunicamycin after incubation with up to 5 μM H1 (C), 20 μM LL37 (D), or 5 μg/mL vancomycin (E) for 60 min. Data are from five independent experiments presented as the mean ± SEM. Statistical significance between WT and the highest concentration of H1, LL37, or vancomycin used was determined by one-way ANOVA with Dunnett's multiple comparison (****$p \leq 0.0001$).

(F) Quantification of metabolic activity by Alamar blue conversion of MRSA exposed to the indicated concentrations of purified WTAs prior to incubation with 5 μM H1 for 60 min. Data are from three independent experiments presented as the mean ± SEM. Statistical significance was determined between control and 250 μg/mL WTAs by a two-sided t test. (*$p \leq 0.05$).

(G) Equilibrium dissociation constant (K_D) of H1 binding to WTAs was determined through microscale thermophoresis.

(H) Metabolic activity of *tarO* and *tarA* mutants transformed with empty vector (ev) or with the expression of *tarO* or *tarA* gene after 60-min incubation with 1 μM H1. Data are from three independent experiments presented as the mean ± SEM. Statistical significance was determined by one-way ANOVA with Dunnett's multiple comparison (****$p \leq 0.0001$).

(I) Metabolic activity of the *ltaA* and *ypfP* mutants after 60-min incubation with H1. Data are from three independent experiments presented as the mean ± SEM. Statistical significance was determined by one-way ANOVA with Dunnett's multiple comparison (*$p \leq 0.05$; **$p \leq 0.01$).

which block cell division, confer resistance to H1. This confirms that both cell division and the PMF are necessary for H1-mediated killing, and disrupting either one makes MRSA resistant to H1.

During cell division, *S. aureus* splits into two daughter cells through the formation of a septum, a process that requires the synthesis of a new plasma membrane and cell wall.[59] WTAs are specifically synthesized at the septum formation site,[48] and we observed clear binding of H1 at these septa (Figure 2A). We hypothesize that the septa are MRSA's Achilles heel, as has been suggested by others[60]; H1 binding to, and disruption of, the membrane may be facilitated by the extreme curvature of the membrane at these distal sites. Upon permeabilizing the cell membrane, H1 enters the cell (Figures 2A and 2D) and colocalizes with *S. aureus* DNA. H1 binding to DNA may contribute to the killing, although we cannot exclude that factors involved in facilitating H1 entry into MRSA, such as disintegration of the cell membrane, are the actual causal factors in MRSA killing. We employed several approaches to separate the possible contribution of DNA binding from that of membrane permeabilization, for example through the transfection of MRSA with an H1-expressing plasmid or through electroporation of H1 into nondividing MRSA, but did not succeed in introducing H1 directly into the cytoplasm of MRSA.

Within our evolution experiments, we identified different founder mutations in all three evolved cultures. The frameshift mutation in *tarA* likely encodes a nonfunctional protein, but the mutations in *pdhB*/*pdhC* and *atpG* resulted in single amino acid substitutions. As both PdhB/PdhC and AtpG are part of a larger multi-subunit protein complex, these missense mutations may affect either protein activity or their regulation. Although we could recapitulate H1 resistance by creating a knockout of *tarA* and *pdh* operon components, we did not observe this for the *atpG* knockout, suggesting that the resistance phenotype is likely not caused by a loss of AtpG function but perhaps by an increase in activity, a change in regulation, or another change of function. Interestingly, RT-qPCR results indicate a reduced expression of the mutant *atpG*, and increased expressions of the mutant *pdhC* and possibly mutant *pdhB*, in the evolved H1-resistant strains (Figures S3E and S3F). These data highlight the importance of ATP synthase and the PDHC in *S. aureus* physiology, and we hypothesize that mutations in the *tcy* operon and *vraG* emerged to compensate for the malfunctions of ATP synthase and the PDHC. Indeed, we also interrogated the secondary mutations identified in the three evolved cultures by generating knockouts of *tcyABC*, *vraG*, and *codY*. By themselves we did not observe any increase in H1 resistance, suggesting they may be advantageous to sustaining the phenotype introduced by the founder mutation. Importantly, we did not notice a difference in growth dynamics for any of the evolved cultures. This may be explained by our experimental setup, which in addition to H1 resistance selects for the mutant that divides the fastest and can become dominant during subculturing.

The three independent evolution experiments all generated a unique resistance to H1. It would be interesting to discover how many different answers to the problem evolution could come up with. Repeats of the same evolution experiment may not only shed more light on the mechanism of action of H1 killing but may also provide a tool to identify essential pathways required for resistance. In light of the current antibiotic crisis, this could facilitate the design of therapies that in combination with antibiotic treatment would selectively target keystones of antibiotic resistance. Furthermore, the observation that H1 targets metabolically active dividing MRSA is in line with the observation that bacteria in stationary phase are more resistant to the antimicrobial activity of a range of AMPs.[61]

The antimicrobial activity of histones toward *S. aureus* has been identified in several publications.[15,30,35,62] In these studies, part of the activity was attributed to the membrane-destabilizing activity of histones, although these studies were often performed in nonphysiological media, and the presence of magnesium and calcium are known to inhibit the antimicrobial activity of histones.[17] In the same study, the depolarizing activity of H2A is described in detail, but H2A alone is unable to permeabilize and enter the bacterial cytoplasm without the synergistic pore-forming activity of LL37. This synergy allowed H2A to bind to bacterial DNA. In the current study, under physiological conditions we did not detect noticeable killing of MRSA by the core histones H2A, H2B, H3, and H4. We found H1 to be the main MRSA killer; H1 permeabilized the membrane, entered the bacterial cytoplasm and bound to bacterial DNA in the absence of other AMPs. It would be interesting to analyze the different molecular structures needed to drive the membrane depolarization, permeabilization, and DNA binding to increase our understanding of the structure-activity relationship of AMPs.

Histones are unlikely to come into contact with pathogens during host homeostasis. However, during inflammation, NETs generated by neutrophils expose chromatin, including H1, which contributes to the antimicrobial activity of NETs. More recently, H1 has also been identified in murine lipid droplets in the liver, and these lipid droplets may provide another means for the host to leverage the antimicrobial activity of H1 in response to bacterial challenge.[9,63]

Limitations of the study

On the host side, a limitation of the study is the lack of genetic tools to study H1. There are 11 subtypes of H1 in both mice and human, five of which are required for somatic replication.[24] Since there are no animals, or even cells, that lack all five H1 subtypes, it is not possible to genetically test the contribution of H1 in bacterial killing *in vivo*. On the bacterial side, as mentioned above, several of the genes we identified that confer susceptibility to H1 in MRSA are required for a robust infection because of their function in metabolism or in the building of the cell wall. This is in accordance with the concept that the innate immune system targets essential structures in microbes but complicates the disambiguation of the *in vivo* function of the genes identified in this report. Furthermore, this aligns with the limitation of the evolution experiment, in which mutants with resistance to H1 are selected, but those that are least affected in growth rate as a result of that mutation, and in the absence of additional selection pressure, are likely to outgrow other mutants and become dominant in the culture.

Conclusions

We provide evidence through two unbiased approaches that H1 targets WTAs of metabolically active and dividing cells, which

facilitates the permeabilization of the membrane and binding of H1 intracellularly to DNA (graphical abstract). As far as we know, the targeting of WTAs is a distinctive feature of H1 and has not been observed for other AMPs. Therefore, this part of the mechanism of action of H1 is selective to gram-positive bacteria. Our data are in line with observations by others that suggest specificity of certain AMPs for different pathogens under diverse physiological contexts. Understanding how AMPs work is essential in understanding host-pathogen interactions and might lead to the design of novel therapeutic approaches in the face of increasing antibiotic resistance.

RESOURCE AVAILABILITY

Lead contact

Further information and requests for resources and reagents should be directed to and will be fulfilled by the lead contact, Arturo Zychlinsky (zychlinsky@mpiib-berlin.mpg.de).

Materials availability

Reagents and strains used and/or generated in this study will be made available upon reasonable request after completion of a materials transfer agreement. Shipping fees might also be required.

Data and code availability

- This paper does not report original code.
- All data reported in this paper will be shared by the lead contact upon request.
- Any additional information required to reanalyze the data reported in this paper is available from the lead contact upon request.

ACKNOWLEDGMENTS

We thank members of the Torres laboratory for insightful discussions. We thank Ashley L. Dumont and Irnov Irnov for hemolysis scoring of the clinical isolates. This work was supported in part by the Max Planck Society; the NIH-National Institute of Allergy and Infectious Diseases award numbers R01s AI099394, AI105129, and AI140754 (V.J.T.); and Burroughs Wellcome Fund (V.J.T.). The NYU Langone Health Genome Technology Center (RRID: SCR_017929) was partially supported by the Cancer Center support grant P30CA016087 from the NIH-National Cancer Institute.

AUTHOR CONTRIBUTIONS

Conceptualization, G.M., V.J.T., and A.Z.; methodology, G.M. and X.Z.; formal analysis, G.M., X.Z., and C.J.H.; investigation, G.M., X.Z., D.Č., K.A.L., M.L., C.G., and V.B.; resources, D.H.; writing – original draft, G.M.; writing – review & editing, G.M., V.J.T., and A.Z.; funding acquisition, V.J.T. and A.Z.; supervision, G.M., V.J.T., and A.Z.

DECLARATION OF INTERESTS

V.J.T. is an inventor on patents and patent applications filed by New York University, which are currently under the commercial license to Janssen Biotech Inc. (JBIO). JBIO provides research funding and other payments associated with an exclusive licensing agreement to V.J.T. The work presented herein is unrelated to these patents.

STAR★METHODS

Detailed methods are provided in the online version of this paper and include the following:

SUPPLEMENTAL INFORMATION

Supplemental information can be found online at https://doi.org/10.1016/j.celrep.2024.114969.

Received: March 11, 2024
Revised: October 6, 2024
Accepted: October 23, 2024
Published: November 14, 2024

REFERENCES

1. Kornberg, R.D. (1974). Chromatin structure: a repeating unit of histones and DNA. Science *184*, 868–871.
2. Miller, B.F., Abrams, R., Dorfman, A., and Klein, M. (1942). Antibacterial properties of protamine and histone. Science *96*, 428–430.
3. HIRSCH, J.G. (1958). Bactericidal action of histone. J. Exp. Med. *108*, 925–944.
4. Richards, R.C., O'Neil, D.B., Thibault, P., and Ewart, K.V. (2001). Histone H1: an antimicrobial protein of Atlantic salmon (Salmo salar). Biochem. Biophys. Res. Commun. *284*, 549–555.
5. Kawasaki, H., Isaacson, T., Iwamuro, S., and Conlon, J.M. (2003). A protein with antimicrobial activity in the skin of Schlegel's green tree frog Rhacophorus schlegelii (Rhacophoridae) identified as histone H2B. Biochem. Biophys. Res. Commun. *312*, 1082–1086.
6. De Zoysa, M., Nikapitiya, C., Whang, I., Lee, J.S., and Lee, J. (2009). Abhisin: a potential antimicrobial peptide derived from histone H2A of disk abalone (Haliotis discus discus). Fish Shellfish Immunol. *27*, 639–646.
7. Nikapitiya, C., Dorrington, T., and Gómez-Chiarri, M. (2013). The role of histones in the immune responses of aquatic invertebrates. ISJ *10*, 94–101.
8. Fernandes, J.M.O., Kemp, G.D., Molle, M.G., and Smith, V.J. (2002). Antimicrobial properties of histone H2A from skin secretions of rainbow trout, Oncorhynchus mykiss. Biochem. J. *368*, 611–620.
9. Anand, P., Cermelli, S., Li, Z., Kassan, A., Bosch, M., Sigua, R., Huang, L., Ouellette, A.J., Pol, A., Welte, M.A., and Gross, S.P. (2012). A novel role for lipid droplets in the organismal antibacterial response. Elife *1*, e00003.
10. Brinkmann, V., Reichard, U., Goosmann, C., Fauler, B., Uhlemann, Y., Weiss, D.S., Weinrauch, Y., and Zychlinsky, A. (2004). Neutrophil Extracellular Traps Kill Bacteria Brinkmann. Science *303*, 1532–1535.

11. Rose-Martel, M., Kulshreshtha, G., Ahferom Berhane, N., Jodoin, J., and Hincke, M.T. (2017). Histones from Avian Erythrocytes Exhibit Antibiofilm activity against methicillin-sensitive and methicillin-resistant Staphylococcus aureus. Sci. Rep. *7*, 45980.

12. Wang, B., Gu, H.J., Huang, H.Q., Wang, H.Y., Xia, Z.H., and Hu, Y.H. (2020). Characterization, expression, and antimicrobial activity of histones from Japanese flounder Paralichthys olivaceus. Fish Shellfish Immunol. *96*, 235–244.

13. Fernandes, J.M.O., Molle, G., Kemp, G.D., and Smith, V.J. (2004). Isolation and characterisation of oncorhyncin II, a histone H1-derived antimicrobial peptide from skin secretions of rainbow trout, Oncorhynchus mykiss. Dev. Comp. Immunol. *28*, 127–138.

14. Park, C.B., Kim, M.S., and Kim, S.C. (1996). A novel antimicrobial peptide from Bufo bufo gargarizans. Biochem. Biophys. Res. Commun. *218*, 408–413.

15. Lee, D.Y., Huang, C.M., Nakatsuji, T., Thiboutot, D., Kang, S.A., Monestier, M., and Gallo, R.L. (2009). Histone H4 is a major component of the antimicrobial action of human sebocytes. J. Invest. Dermatol. *129*, 2489–2496.

16. Kawasaki, H., and Iwamuro, S. (2008). Potential roles of histones in host defense as antimicrobial agents. Infect. Disord.: Drug Targets *8*, 195–205.

17. Doolin, T., Amir, H.M., Duong, L., Rosenzweig, R., Urban, L.A., Bosch, M., Pol, A., Gross, S.P., and Siryaporn, A. (2020). Mammalian histones facilitate antimicrobial synergy by disrupting the bacterial proton gradient and chromosome organization. Nat. Commun. *11*, 3888.

18. Marsman, G., Zeerleder, S., and Luken, B.M. (2016). Extracellular histones, cell-free DNA, or nucleosomes: differences in immunostimulation. Cell Death Dis. *7*, e2518.

19. Cramer, T.J., Sinha, R.K., and Griffin, J.H. (2013). Reduction Of Histone H1 Cytotoxicity By Activated Protein C and Its Exosite Variants. Blood *122*, 2334.

20. Alhamdi, Y., Abrams, S.T., Cheng, Z., Jing, S., Su, D., Liu, Z., Lane, S., Welters, I., Wang, G., and Toh, C.H. (2015). Circulating Histones Are Major Mediators of Cardiac Injury in Patients With Sepsis. Crit. Care Med. *43*, 2094–2103.

21. Kawano, H., Ito, T., Yamada, S., Hashiguchi, T., Maruyama, I., Hisatomi, T., Nakamura, M., and Sakamoto, T. (2014). Toxic effects of extracellular histones and their neutralization by vitreous in retinal detachment. Lab. Invest. *94*, 569–585.

22. Xu, J., Zhang, X., Pelayo, R., Monestier, M., Ammollo, C.T., Semeraro, F., Taylor, F.B., Esmon, N.L., Lupu, F., and Esmon, C.T. (2009). Extracellular histones are major mediators of death in sepsis. Nat. Med. *15*, 1318–1321.

23. Chapman, G.E., Hartman, P.G., and Bradbury, E.M. (1976). Studies on the role and mode of operation of the very-lysine-rich histone H1 in eukaryote chromatin. The isolation of the globular and non-globular regions of the histone H1 molecule. Eur. J. Biochem. *61*, 69–75.

24. Hergeth, S.P., and Schneider, R. (2015). The H1 linker histones: multifunctional proteins beyond the nucleosomal core particle. EMBO Rep. *16*, 1439–1453.

25. Bednar, J., Garcia-Saez, I., Boopathi, R., Cutter, A.R., Papai, G., Reymer, A., Syed, S.H., Lone, I.N., Tonchev, O., Crucifix, C., et al. (2017). Structure and Dynamics of a 197 bp Nucleosome in Complex with Linker Histone H1. Mol. Cell *66*, 729.

26. Parseghian, M.H. (2015). What is the role of histone H1 heterogeneity? A functional model emerges from a 50 year mystery. AIMS Biophys. *2*, 724–772. https://doi.org/10.3934/biophy.2015.4.724.

27. Misteli, T., Gunjan, A., Hock, R., Bustin, M., and Brown, D.T. (2000). Dynamic binding of histone H1 to chromatin in living cells. Nature *408*, 877–881.

28. Jacobsen, F., Baraniskin, A., Mertens, J., Mittler, D., Mohammadi-Tabrisi, A., Schubert, S., Soltau, M., Lehnhardt, M., Behnke, B., Gatermann, S., et al. (2005). Activity of histone H1.2 in infected burn wounds. J. Antimicrob. Chemother. *55*, 735–741.

29. Rose, F.R., Bailey, K., Keyte, J.W., Chan, W.C., Greenwood, D., and Mahida, Y.R. (1998). Potential role of epithelial cell-derived histone H1 proteins in innate antimicrobial defense in the human gastrointestinal tract. Infect. Immun. *66*, 3255–3263.

30. Tagai, C., Morita, S., Shiraishi, T., Miyaji, K., and Iwamuro, S. (2011). Antimicrobial properties of arginine- and lysine-rich histones and involvement of bacterial outer membrane protease T in their differential mode of actions. Peptides (NY) *32*, 2003–2009.

31. Kashima, M. (1991). H1 histones contribute to candidacidal activities of human epidermal extract. J. Dermatol. *18*, 695–706.

32. Howell, S.J., Wilk, D., Yadav, S.P., and Bevins, C.L. (2003). Antimicrobial polypeptides of the human colonic epithelium. Peptides (NY) *24*, 1763–1770.

33. Kawasaki, H., Koyama, T., Conlon, J.M., Yamakura, F., and Iwamuro, S. (2008). Antimicrobial action of histone H2B in Escherichia coli: evidence for membrane translocation and DNA-binding of a histone H2B fragment after proteolytic cleavage by outer membrane proteinase T. Biochimie *90*, 1693–1702.

34. Hancock, R.E.W., and Sahl, H.-G. (2006). Antimicrobial and host-defense peptides as new anti-infective therapeutic strategies. Nat. Biotechnol. *24*, 1551–1557.

35. Morita, S., Tagai, C., Shiraishi, T., Miyaji, K., and Iwamuro, S. (2013). Differential mode of antimicrobial actions of arginine-rich and lysine-rich histones against Gram-positive Staphylococcus aureus. Peptides (NY) *48*, 75–82.

36. Marsman, G., von Richthofen, H., Bulder, I., Lupu, F., Hazelzet, J., Luken, B.M., and Zeerleder, S. (2016). DNA and Factor VII-activating protease protect against the cytotoxicity of histones. In Factor VII-Activating Protease: Unraveling the Release and Regulation of Dead Cell Nuclear DAMPs, *Chapter 5*.

37. Chen, R., Kang, R., Fan, X.-G., and Tang, D. (2014). Release and activity of histone in diseases. Cell Death Dis. *5*, e1370.

38. Gardete, S., and Tomasz, A. (2014). Mechanisms of vancomycin resistance in Staphylococcus aureus. J. Clin. Invest. *124*, 2836–2840.

39. Walters, M.S., Eggers, P., Albrecht, V., Travis, T., Lonsway, D., Hovan, G., Taylor, D., Rasheed, K., Limbago, B., and Kallen, A. (2015). Vancomycin-resistant staphylococcus aureus - Delaware. MMWR Morb. Mortal. Wkly. Rep. *64*, 1056.

40. Chambers, H.F., and DeLeo, F.R. (2009). Waves of resistance: Staphylococcus aureus in the antibiotic era. Nat. Rev. Microbiol. *7*, 629–641.

41. Deckers-Hebestreit, G., and Altendorf, K. (1996). The F0F1-type ATP synthases of bacteria: structure and function of the F0 complex. Annu. Rev. Microbiol. *50*, 791–824.

42. Liu, L., Beck, C., Nøhr-Meldgaard, K., Peschel, A., Kretschmer, D., Ingmer, H., and Vestergaard, M. (2020). Inhibition of the ATP synthase sensitizes Staphylococcus aureus towards human antimicrobial peptides. Sci. Rep. *10*, 11391.

43. Mackieh, R., Al-Bakkar, N., Kfoury, M., Roufayel, R., Sabatier, J.M., and Fajloun, Z. (2023). Inhibitors of ATP Synthase as New Antibacterial Candidates. Antibiotics *12*, 650.

44. Fey, P.D., Endres, J.L., Yajjala, V.K., Widhelm, T.J., Boissy, R.J., Bose, J.L., and Bayles, K.W. (2013). A genetic resource for rapid and comprehensive phenotype screening of nonessential Staphylococcus aureus genes. mBio *4*, e00537. https://doi.org/10.1128/mBio.00537-12.

45. Swoboda, J.G., Campbell, J., Meredith, T.C., and Walker, S. (2010). Wall teichoic acid function, biosynthesis, and inhibition. Chembiochem *11*, 35–45.

46. Xia, G., Kohler, T., and Peschel, A. (2010). The wall teichoic acid and lipoteichoic acid polymers of Staphylococcus aureus. Int. J. Med. Microbiol. *300*, 148–154.

47. Mann, P.A., Müller, A., Wolff, K.A., Fischmann, T., Wang, H., Reed, P., Hou, Y., Li, W., Müller, C.E., Xiao, J., et al. (2016). Chemical Genetic Analysis and Functional Characterization of Staphylococcal Wall Teichoic Acid

2-Epimerases Reveals Unconventional Antibiotic Drug Targets. PLoS Pathog. *12*, e1005585.

48. Rahman, M.M., Hunter, H.N., Prova, S., Verma, V., Qamar, A., and Golemi-Kotra, D. (2016). The Staphylococcus aureus methicillin resistance factor FmtA is a D-amino esterase that acts on teichoic acids. mBio *7*, 1–11.
49. Brown, S., Xia, G., Luhachack, L.G., Campbell, J., Meredith, T.C., Chen, C., Winstel, V., Gekeler, C., Irazoqui, J.E., Peschel, A., and Walker, S. (2012). Methicillin resistance in Staphylococcus aureus requires glycosylated wall teichoic acids. Proc. Natl. Acad. Sci. USA *109*, 18909–18914.
50. Schlag, M., Biswas, R., Krismer, B., Kohler, T., Zoll, S., Yu, W., Schwarz, H., Peschel, A., and Götz, F. (2010). Role of staphylococcal wall teichoic acid in targeting the major autolysin Atl. Mol. Microbiol. *75*, 864–873.
51. Campbell, J., Singh, A.K., Santa Maria, J.P., Jr., Kim, Y., Brown, S., Swoboda, J.G., Mylonakis, E., Wilkinson, B.J., and Walker, S. (2011). Synthetic lethal compound combinations reveal a fundamental connection between wall teichoic acid and peptidoglycan biosyntheses in Staphylococcus aureus. ACS Chem. Biol. *6*, 106–116.
52. Biswas, R., Martinez, R.E., Göhring, N., Schlag, M., Josten, M., Xia, G., Hegler, F., Gekeler, C., Gleske, A.K., Götz, F., et al. (2012). Proton-binding capacity of staphylococcus aureus wall teichoic acid and its role in controlling autolysin activity. PLoS One *7*, e41415.
53. Koprivnjak, T., Weidenmaier, C., Peschel, A., and Weiss, J.P. (2008). Wall Teichoic Acid Deficiency in Staphylococcus aureus Confers Selective Resistance to Mammalian Group IIA Phospholipase A2 and Human β-Defensin 3. Infect. Immun. *76*, 2169–2176.
54. Winstel, V., Kühner, P., Salomon, F., Larsen, J., Skov, R., Hoffmann, W., Peschel, A., and Weidenmaier, C. (2015). Wall Teichoic Acid Glycosylation Governs Staphylococcus aureus Nasal. Mol. Biol. *6*, e00632.
55. Grosser, M.R., Paluscio, E., Thurlow, L.R., Dillon, M.M., Cooper, V.S., Kawula, T.H., and Richardson, A.R. (2018). Genetic requirements for Staphylococcus aureus nitric oxide resistance and virulence. PLoS Pathog. *14*, e1006907.
56. Bakker, E.P., and Mangerich, W.E. (1981). Interconversion of components of the bacterial proton motive force by electrogenic potassium transport. J. Bacteriol. *147*, 820–826.
57. Farha, M.A., Verschoor, C.P., Bowdish, D., and Brown, E.D. (2013). Collapsing the proton motive force to identify synergistic combinations against staphylococcus aureus. Chem. Biol. *20*, 1168–1178.
58. Singh, V.K., Sirobhushanam, S., Ring, R.P., Singh, S., Gatto, C., and Wilkinson, B.J. (2018). Roles of pyruvate dehydrogenase and branched-chain α-keto acid dehydrogenase in branched-chain membrane fatty acid levels and associated functions in Staphylococcus aureus. J. Med. Microbiol. *67*, 570–578.
59. Zhou, X., Halladin, D.K., Rojas, E.R., Koslover, E.F., Lee, T.K., Huang, K.C., and Theriot, J.A. (2015). Mechanical crack propagation drives millisecond daughter cell separation in Staphylococcus aureus. Science *348*, 574–578.
60. Farha, M.A., Leung, A., Sewell, E.W., D'Elia, M.A., Allison, S.E., Ejim, L., Pereira, P.M., Pinho, M.G., Wright, G.D., and Brown, E.D. (2013). Inhibition of WTA synthesis blocks the cooperative action of pbps and sensitizes MRSA to β-lactams. ACS Chem. Biol. *8*, 226–233.
61. Reygaert, W.C. (2018). An overview of the antimicrobial resistance mechanisms of bacteria. AIMS Microbiol. *4*, 482–501.
62. Pietrocola, G., Nobile, G., Alfeo, M.J., Foster, T.J., Geoghegan, J.A., De Filippis, V., and Speziale, P. (2019). Fibronectin-binding protein B (FnBPB) from Staphylococcus aureus protects against the antimicrobial activity of histones. J. Biol. Chem. *294*, 3588–3602.
63. Bosch, M., Sánchez-Álvarez, M., Fajardo, A., Kapetanovic, R., Steiner, B., Dutra, F., Moreira, L., López, J.A., Campo, R., Marí, M., et al. (2020). Mammalian lipid droplets are innate immune hubs integrating cell metabolism and host defense. Science *370*, eaay8085. https://doi.org/10.1126/science.aay8085.
64. Adhikari, R.P., Arvidson, S., and Novick, R.P. (2007). A nonsense mutation in agrA accounts for the defect in agr expression and the avirulence of Staphylococcus aureus 8325-4 traP::kan. Infect. Immun. *75*, 4534–4540.
65. Kenny, E.F., Herzig, A., Krüger, R., Muth, A., Mondal, S., Thompson, P.R., Brinkmann, V., Bernuth, H.v., and Zychlinsky, A. (2017). Diverse stimuli engage different neutrophil extracellular trap pathways. Elife *6*, e24437.
66. Schindelin, J., Arganda-Carreras, I., Frise, E., Kaynig, V., Longair, M., Pietzsch, T., Preibisch, S., Rueden, C., Saalfeld, S., Schmid, B., et al. (2012). Fiji: An open-source platform for biological-image analysis. Nat. Methods *9*, 676–682.
67. Peters, P.J., Bos, E., and Griekspoor, A. (2006). Cryo-Immunogold Electron Microscopy. Curr. Protoc. Cell Biol. *Chapter 4*, Unit 4.7. https://doi.org/10.1002/0471143030.cb0407s30.
68. Slot, J.W., Geuze, H.J., Gigengack, S., Lienhard, G.E., and James, D.E. (1991). Immuno-localization of the insulin regulatable glucose transporter in brown adipose tissue of the rat. J. Cell Biol. *113*, 123–135.
69. Bankhead, P., Loughrey, M.B., Fernández, J.A., Dombrowski, Y., McArt, D.G., Dunne, P.D., McQuaid, S., Gray, R.T., Murray, L.J., Coleman, H.G., et al. (2017). QuPath: Open source software for digital pathology image analysis. Sci. Rep. *7*, 16878. https://doi.org/10.1038/s41598-017-17204-5.
70. Wick, R.R., Judd, L.M., Gorrie, C.L., and Holt, K.E. (2017). Unicycler: Resolving bacterial genome assemblies from short and long sequencing reads. PLoS Comput. Biol. *13*, e1005595.
71. Seemann, T. (2014). Prokka: rapid prokaryotic genome annotation. Bioinformatics *30*, 2068–2069.
72. Langmead, B., and Salzberg, S.L. (2012). Fast gapped-read alignment with Bowtie 2. Nat. Methods *9*, 357–359.
73. Benjamin, D., Sato, T., Cibulskis, K., Getz, G., Stewart, C., and Lichtenstein, L. (2019). Calling Somatic SNVs and Indels with Mutect2. Preprint at bioRxiv. https://doi.org/10.1101/861054.
74. Cingolani, P., Platts, A., Wang, L.L., Coon, M., Nguyen, T., Wang, L., Land, S.J., Lu, X., and Ruden, D.M. (2012). A program for annotating and predicting the effects of single nucleotide polymorphisms, SnpEff: SNPs in the genome of Drosophila melanogaster strain w1118; iso-2; iso-3. Fly *6*, 80–92.
75. Boles, B.R., Thoendel, M., Roth, A.J., and Horswill, A.R. (2010). Identification of genes involved in polysaccharide-independent Staphylococcus aureus biofilm formation. PLoS One *5*, e10146.
76. Chen, J., Yoong, P., Ram, G., Torres, V.J., and Novick, R.P. (2014). Single-copy vectors for integration at the SaPI1 attachment site for Staphylococcus aureus. Plasmid *76*, 1–7.
77. Schuster, C.F., Howard, S.A., and Gründling, A. (2019). Use of the counter selectable marker PheS* for genome engineering in Staphylococcus aureus. Microbiology (N. Y.) *165*, 572–584.
78. Torres, V.J., Stauff, D.L., Pishchany, G., Bezbradica, J.S., Gordy, L.E., Iturregui, J., Anderson, K.L., Dunman, P.M., Joyce, S., and Skaar, E.P. (2007). A Staphylococcus aureus regulatory system that responds to host heme and modulates virulence. Cell Host Microbe *1*, 109–119.
79. Kho, K., and Meredith, T.C. (2018). Extraction and Analysis of Bacterial Teichoic Acids. Bio. Protoc. *8*, e3078.

STAR★METHODS

KEY RESOURCES TABLE

REAGENT or RESOURCE	SOURCE	IDENTIFIER
Antibodies		
Anti-histone H1 (G1)	Santa Cruz Biotechnology	sc-393530
5/15 nm gold-labeled goat anti-biotin	British Biocell	Custom made
Rabbit polyclonal anti-Staphylococcus aureus protein A	Abcam	ab20920; RRID:AB_445913
6/12/18 nm gold-labeled goat anti-rabbit	Jackson Immuno Research	111-195-144; RRID:AB_2338015 111-205-144; RRID:AB_2338016 111-215-144; RRID:AB_2338017
6/12/18 nm gold-labeled goat anti-mouse	Jackson Immuno Research	115-195-146; RRID:AB_2338728 115-205-146; RRID:AB_2338733 115-215-146; RRID:AB_2338738
Anti-dsDNA (ANA123)	Sanquin	–
Bacterial and virus strains		
See Table S3	See Table S3	–
Nebraska Transposon Mutant Library	University of Nebraska Medical Center	–
Biological samples		
Staphylococcus aureus-infected patient abscess samples	Dr. Daniel Humme	–
Chemicals, peptides, and recombinant proteins		
Purified Histone H1	Merck Millipore	14–155
Recombinant histone H2A	New England Biolabs	M2502
Recombinant histone H2B	New England Biolabs	M2505
Recombinant histone H3.3	New England Biolabs	M2507
Recombinant histone H4	New England Biolabs	M2504
H1.2 N-terminal tail	Pepscan	–
H1.2 C-terminal tail	Pepscan	–
H1.2 C-terminal tail scrambled	Pepscan	–
H1.2 Globular domain	Pepscan	–
CAP18	Anaspec	AS-61307
Cecropin	Anaspec	AS-24009
Dermcidin	Anaspec	AS-63713
HNP1	Anaspec	AS-60743
Indolicidin	Anaspec	AS-60999
LL37	Anaspec	AS-61302
Magainin I	Anaspec	AS-20791
Magainin II	Anaspec	AS-20639
PMA	Sigma-Aldrich	P1585
Alexa Fluor 488/647	Invitrogen	A20181/A20186
EZ-Link™ NHS-LC-Biotin	Thermo Scientific	21336
AlamarBlue	Invitrogen	DAL1100
DiOC2,3	Invitrogen	D14730
Hoechst 33258	Sigma Aldrich	94403
Wheat germ agglutinin-AlexaFluor 555	Invitrogen	W32464
Streptavidin-AlexaFluor 488	Invitrogen	S11223
RPMI 1640 medium, without Phenol Red, without Sodium Bicarbonate	BioWest	P08880/

(*Continued on next page*)

Continued

REAGENT or RESOURCE	SOURCE	IDENTIFIER
Seahorse XF RPMI medium, without Phenol Red, without Sodium Bicarbonate, without glucose	Agilent Technologies	103681100
Histopaque 1119	Sigma-Aldrich	11191
Percoll	GE Healthcare Life Sciences	GE17-0891-02
Critical commercial assays		
ATP quantification kit	Thermo Fischer Scientific	A22066
RNAeasy	Qiagen	74104
RNase-Free DNase Set	Qiagen	79254
High-Capacity cDNA Reverse Transcription Kit	Applied Biosystems	4368814
Oligonucleotides		
See Table S4	–	–
Software and algorithms		
Graphpad Prism V 9.01	–	–
Bowtie2	–	–
R statistical environment	–	–

EXPERIMENTAL MODEL AND SUBJECT DETAILS

Ethics statement and patient samples

Blood samples from healthy individuals were obtained under the approval and guidelines of the Charité ethics committee (EA1/0104/06). Pus samples from *Staphylococcus aureus*-infected patients were obtained under the approval and guidelines of the Charité ethics committee (EA2/003/019). Informed consent was obtained from all subjects. Patient I was suffering from hidradenitis suppurativa and pus was collected from a skin abscess. Patient II pus sample was drawn directly from a skin abscess in the right groin.

METHOD DETAILS

Bacterial strains, culture conditions and preparation

The USA300 community-acquired methicillin-resistant *Staphylococcus aureus* strain WI-2335 (ST8, CC8) (Sanjay K. Shukla lab, Marshfield Clinic, Wisconsin, United States) was used in all experiments except for the transposon screen and complementation studies (see below). The clinical isolates and strains used for the complementation studies are listed in Table S3. Cultures were cryopreserved in TSB (Carl Roth) or RPMI (BioWest) supplemented with 10% glycerol (VWR Life Science) at −80°C. To culture bacteria, 5mL of TSB was inoculated and grown overnight at 37 °C at 180 rpm in an orbital shaker. Bacteria were passaged into fresh TSB and incubated for 2h at 37 °C at 180 rpm until the culture reached mid-logarithmic phase. Bacteria were harvested by centrifugation for 5 min at 2000 x g, washed twice with RPMI 1640 or Seahorse XF RPMI medium supplemented with 5mM HEPES pH7.4 and supplemented with or without glucose and adjusted to OD_{600} = 0.1. MRSA cultures generated in the evolution experiments were cultured in RPMI at 37 °C at 180 rpm instead of in TSB. In experiments, the cultures were used at a final OD_{600} of 0.05, which equated to roughly 50 x 10^6/mL.

Determination of hemolysis activity

The hemolysis activity of clinical isolates was determined using methods as described.[64] Strains were streaked on sheep blood agar (BD) with RN4220 and incubated for 24 h at 37°C. The hemolytic zone was blindly scored by three individuals separately and averaged (0-no hemolysis, 3-significant hemolysis). Of note, when significant beta-hemolysis was present in a strain, alpha-hemolysis was not scored (indicated as n/a). The color of the colonies were scored similarly (0-white, 3-yellow).

Antimicrobial compounds

Purified histone H1 protein (14–155, Merck Millipore), recombinant histone H2A, H2B, H3, and H4 (New England Biolabs), CAP18, Cecropin, dermcidin, HNP1, Indolicidin, LL37, Magainin I and II (Anaspec) were used at 5 μM unless otherwise indicated. For imaging purposes, histone H1 was labeled with biotin or with an Alexa Fluor 647 (Invitrogen) at a labeling ratio of 4 labels to 1 histone H1 according to the manufacturers' instructions. Vancomycin and Daptomycin were purchased from Sigma-Aldrich.

Bacterial metabolic activity

Bacteria were incubated in triplicate in RPMI (supplemented with or without 5% heat-inactivated human serum) with the antimicrobial compound of interest at 37°C in a 96-well flat bottom plate for 1 h, followed by 1:10 addition of alamarBlue (Invitrogen) and an additional 1 h incubation. Fluorescence was measured using 540 nm excitation and 590 nm emission wavelengths in a Fluoroskan Ascent plate reader (Thermo Labsystems). Bacteria incubated in medium alone were used as a negative control, whilst 0.5% Triton X-100 (Sigma-Aldrich) + 10 μg/mL Lysostaphin (Sigma-Aldrich) was used as a positive control. For measurement of background signal, wells with medium alone + alamarBlue were used. Values were adjusted for the background signal and normalized to the positive and negative control samples.

Bacterial killing assay

Bacteria were incubated in triplicate in RPMI (supplemented with or without 5% heat-inactivated fetal calf serum) with the antimicrobial compound of interest at 37°C in a 96-well flat bottom plate for 2 h. Samples were serially diluted 1:10 into PBS and 10 μL droplets were pipetted onto pre-warmed TSA plates, allowed to dry in, and incubated overnight at 37°C. Colony forming units (CFU) were counted in the droplets with more than 4, and fewer than 50 colonies.

Isolation of neutrophils from human blood

Neutrophils were isolated from the peripheral blood of healthy adult donors as described previously.[65] In short, EDTA-blood was layered on an equal volume of Histopaque 1119 (Sigma-Aldrich), centrifuged for 20 min at 800 x g and the third pink colored layer consisting mainly of neutrophils was collected. Subsequently, the cell suspension was washed with DPBS supplemented with 0.1% HSA, centrifuged for 10 min at 300 x g, and resuspended in 2 mL of DPBS with 0.1% HAS. Cells were layered on a 85-65% discontinuous gradient of Percoll (GE Healthcare Life Sciences). After 20 min centrifugation at 800 x g, the neutrophils were collected from the interface between the 65% and 75% Percoll layers. Neutrophils were washed once more with DPBS with 0.1% HSA and counted with a CASY1 cell counter (Schärfe system).

NETs killing of MRSA

Isolated neutrophils were centrifuged for 10 min at 300 x g and resuspended in RPMI supplemented with 10% human serum (Sigma-Aldrich). 10^6 neutrophils were seeded in a flat-bottom 96 well plate, and NETosis was induced with 200 nM phorbol 12-myristate 13-acetate (PMA, Sigma-Aldrich) for 3h at 37°C. To inhibit the antimicrobial activity of histone H1, 30 μg/mL of anti-histone H1 (G-1 clone, Santa Cruz Biotechnology) was added to a subset of samples. As a control, an IgM isotype control (R&D Systems) was used. WT MRSA culture in RPMI with 10% human serum was added to each well at a multiplicity of infection of 0.1, and the plate was incubated for 2 h at 37°C. NETs were treated with 2U micrococcal nuclease from *S. aureus* (MNase, Sigma-Aldrich) for 10 min at RT and samples were 1:10 serially diluted in DPBS and plated on trypticase soy agar plates. The plates were incubated at 37 °and CFU were counted the next day.

Growth profiles

Bacterial cultures were diluted to OD_{600} = 0.05 and transferred to a flat-bottom 96-well plate. The plate was immediately placed into a pre-heated (37°C) plate reader Synergy HTX (BioTek) or Epoch (BioTek) and incubated overnight at 37°C with orbital shaking prior to each measurement. Absorbance at OD_{600} was measured every 20 min for 22 h.

Membrane potential assay

MRSA (3×10^{8}) was incubated with 5μM DiOC2,3 in RPMI supplemented with 0.05% HSA and 1% DMSO for 10 min at 37°C. Then, fluorescence measurements (Excitation: 485, Emission: 538 and 620 nm), were started in 5 min intervals in a Synergy HTX or Epoch (Biotek) at 37°C. A baseline was determined during the first 15 min, followed by the incubation with 8μg/mL Oligomycin, 5μM Valinomcyin or buffer for 15 min and the addition of 5μM H1 or 20μM LL37. As a positive control 10μM CCCP was used to collapse the membrane potential. The ratio of 620 nm over 538 nm fluorescence was determined as a readout of the membrane potential.

ATP assay

ATP levels released upon histone H1 incubation were determined using a commercial ATP assay kit, according to the manufacturers' instructions (A22066, Thermo Fischer Scientific). MRSA was incubated with H1 for the indicated times at 37°C, spun down for 5 min at 2000 xg and supernatant was collected. To determine the total amount of ATP present in MRSA at the indicated times, identical samples were prepared in parallel and subjected to 2 × 30s lysis using 0.1 mm silica spheres (MP Bio) in a Precellys Evolution homogenizer (Bertin instruments) at 6800 rpm. The ATP amounts in the samples were normalized to the lysed control.

Flow cytometry

MRSA was incubated in the presence or absence of Alexa Fluor 647-labeled H1 for 15–120 min at 37°C. Subsequently, bacteria were washed twice with RPMI, fixed with 4% paraformaldehyde (Electron Microscopy Sciences) in RPMI for 15 min at RT, and washed twice with DPBS (Gibco). The fluorescence of the samples was measured on the flow cytometer CytoFLEX (BeckMan Coulter). All results were analyzed using the FlowJo software v10 (Becton-Dickinson).

Fluorescence cell sorting

MRSA was incubated with 1μM AlexaFluor647-labeled H1 for 30 min in RPMI at 37°C. Bacteria with surface-bound H1 (dim) and bacteria permeabilized with H1 (bright) were sorted by FACS using a BD FACSAria II.

Confocal microscopy

MRSA in RPMI was transferred to IBIDI-slides with 8 imaging chambers (IBIDI) and incubated with Alexa Fluor 647-labeled H1 for 15–60 min at 37°C. Bacteria were spun down onto the slide for 5 min at 2000 x g, and carefully washed three times with DPBS. All images were acquired using a confocal laser scanning microscope Leica TCS SP8 (Leica Microsystems) with an objective HC Plan-Apochromat 63×/1.3 glycerine (Zeiss), and a 15x zoom. Same settings were used each time a repeated condition was imaged, and Fiji was used to process the acquired images.[66]

Transmission electron microscopy

Immunogold electron microscopy and confocal microscopy of ultrathin/semithin Cryosections

Bacteria were incubated with 1 μM (biotinylated)-H1 for 1 h at 37°C, washed once with DPBS and fixed with 4% PFA +0.05% glutaraldehyde. For pus samples, samples were collected from the clinic within 4 h of sampling and were fixed with 4% PFA +0.05% glutaraldehyde for 1 h. Samples were gelatin-embedded and infiltrated with 2.3M Sucrose according to the method described previously.[67]

For TEM analysis, ultrathin sections were cut at −110°C with an RMC MTX/CRX cryo-ultramicrotome (Boeckeler Instruments Inc., Tucson AZ, USA) transferred to carbon- and pioloform-coated EM-grids and blocked with 0.3% BSA, 0.01M Glycin, 3% CWFG in PBS. The sections were incubated with appropriate dilutions in the same buffer of mouse IgM monoclonal antibody directed against H1 (G-1), 5nm gold-labeled goat monoclonal antibody directed against biotin (British Bio Cell), a rabbit polyclonal antibody directed against *S. aureus* protein A or a mouse monoclonal antibody directed against double-stranded DNA (dsDNA) (ANA123, Sanquin). Secondary antibody-incubations were carried out with goat-*anti*-rabbit, goat-*anti*-mouse antibodies coupled to 18 nm, 12 nm or 6 nm gold particles (Jackson Immuno Research, West Grove, PA, USA). Specimens were then contrasted and embedded with uranyl-acetate/methyl-cellulose following the method described[68] and analyzed in a Leo 906 transmission electron microscope (Zeiss, Oberkochen, Germany) operated at 100 kV. Images were recorded using a side-mount Morada digital camera (SIS, Münster, Germany).

For confocal analysis, semithin sections were cut at −79°C with an RMC MTX/CRX cryo-ultramicrotome (Boeckeler Instruments Inc., Tucson AZ, USA) transferred to glass coverslips and incubated with Hoechst 33258, wheat germ aglutinin-Alexa Fluor-555 and Streptavidin Alexa Fluor 488. The coverslips were mounted on glass slides with Mowiol and analyzed with a Leica SP8 confocal system. Images were quantified with QuPath software.[69]

Bacterial evolution experiment

An overnight culture of WT MRSA was passaged 1:100 into 2 mL of RPMI, with or without 1 μM of histone H1, and grown overnight at 37°C with shaking at 180 rpm. The next day, the two cultures were passaged in the same way, and the daily subculturing was continued for 14 to 21 days. Resistance to histone H1 was assessed daily with a bacterial killing assay (see above). In addition, a 10% glycerol stock was made daily from each overnight culture and stored at −80°C.

A total of 86 single colonies from three evolution experiments (Experiment 1 and 3: 28 resistant colonies and 10 control colonies; Experiment 2: 6 resistant colonies and 4 control colonies) were sequenced with Illumina NovaSeq 6000 platform at the NYU Langone's Genome Technology Center. The parental WT strain was sequenced with Illumina NovaSeq 6000 and Oxford Nanopore MinION to generate both short and long reads. The WT genome was hybrid-assembled using Unicycler and annotated using Prokka based on proteins in USA300_FPR3757.[70,71] The reads of the clones were mapped to the WT genome using Bowtie2.[72] The differences between resistant and control colonies in each experiment were identified using mutect2 with minimum-allele-fraction of 0.5 and callable-depth of 30.[73] The effects of mutation were predicted using SnpEff[74] and operons were annotated manually based on gene locations and function.

RNA isolation and RT-qPCR

Evolved MRSA cultures were washed twice with PBS and diluted to an OD_{600} of 0.5 in 1 mL. The culture was pelleted, resuspended in RNA later stabilization solution (Invitrogen) and incubated for 1h at RT. Bacteria were lysed with 20 μg/mL of lysostaphin (Sigma-Aldrich) in TE buffer (10 mM Tris, 1 mM EDTA, pH = 8) for 10 min at 37°C. RNA isolation was performed using the RNAeasy mini kit (Qiagen) following the manufacturer's instructions. An additional step was added after the addition of the RLT buffer where the lysate was transferred to a 2 mL Lysing matrix B tube with 0.1 mm silica beads (MP Biomedicals) and disrupted in a Precellys Evolution homogenizer 2 × 30 s at 4500 rpm. On-column DNase I digestion was performed using RNase-Free DNase Set (Qiagen) to remove contaminating DNA. RNA concentration was measured on Nanodrop (Thermo Fisher Scientific) and 100 ng of total RNA was reverse transcribed to cDNA using High-Capacity cDNA Reverse Transcription Kit (Applied Biosystems) with random primers according to the manufacturer's instructions. qPCR was carried out using 1 μL of cDNA and 500 nM of specific primers with the Fast SYBR Green Master Mix (Thermo Fisher Scientific) on the Quant Studio 3 Real-Time PCR System (Applied Biosystems).

Sequences of primers used in this study are listed in Table S4. Expression values were normalized to the housekeeping gene rpoB and relative fold changes over the control were calculated using the $2^{-\Delta\Delta Ct}$ method.

Transposon library screen

Mutants in the Nebraska transposon mutant library were grown overnight in 96-well plates, and subcultured 1:100 in duplicate in the morning at 37°C in the absence or presence of 1μM H1. Metabolic activity was measured as described above. For growth measurements, mutants were incubated for 6 h at 37°C and OD_{600} was determined. 237 mutants with increased or decreased sensitivity to H1 were selected and their metabolic activity and growth determined in triplicate in a second screen. The 80 mutants with highest or lowest sensitivity to H1 were then tested again in triplicate in a tertiary screen and also tested against 50μg/mL LL-37, 1μg/mL vancomycin, or 1μg/mL daptomycin in the same way as for H1.

Generating mutant and complement strains

The transposon insertion mutants of *tarX*, *ychF*, *fmtA*, and *trkA* were generated by transducing the mutations of respective JE2 mutant strains from the Nebraska transposon mutant library into LAC[75] with phage 80α. To complement the phenotypes of these mutants, chromosomal expression of the *tarGBXD* operon, *ychF*, *fmtA*, and *trkA* under the control of the native promoters were achieved using the pJC1111 integration system.[76]

The Δ*atpG*, *ΔtcyABC*, *ΔpdhA*, *ΔpdhB*, *ΔpdhC*, *ΔpdhD*, *ΔvraG*, *ΔtarO*, *ΔtarA*, *ΔcodY* mutants were generated by replacing the respective gene locus in LAC WT with *aad9* gene encoding spectinomycin resistance using the pIMAY* allelic exchange system.[77] The *ΔtarA* and Δ*tarO* mutants were complemented using a hemin-inducible system by cloning the *tarA* or *tarO* gene into the pOS1-*PhrtAB* plasmid.[78]

Microscale thermophoresis

Microscale Thermophoresis experiments were performed on a Monolith (Nanotemper) according to the manufacturer's instructions. Briefly, AF647-labeled histone H1 (20nM) was incubated with the indicated concentrations of WTA in RPMI in Monolith NT.115 MST Premium Coated Capillaries and fluorescence was determined in the red channel.

Wall teichoic acid extraction and SDS-PAGE

WT MRSA and the evolution cultures were grown overnight in 20 mL of TSB. As a control, WT MRSA was incubated with 0.4 μg/mL tunicamycin (Sigma-Aldrich) to block the synthesis of the wall teichoic acids. The isolation of wall teichoic acids was performed as described before.[79] All cultures were washed once with fresh TSB and diluted to the same OD_{600}. Next, the cultures were washed with 30 mL of Buffer 1 (pH 6.5, 50 mM 2-(N-Morpholino) ethanesulfonic acid MES (Sigma-Aldrich) in dH_20), and with 30 mL of Buffer 2 (pH 6.5, 50 mM MES and 4% sodium dodecyl sulfate SDS (Carl Roth) in dH_20). The tubes with cell suspensions were placed in boiling water for 1h and subsequently centrifuged, washed with 1 mL of Buffer 1, and transferred to a 2 mL microtubes which were centrifuged for 1 min at 16 000 x g. The samples were washed with 2 mL of buffers starting with Buffer 2, then Buffer 3 (pH 6.5, 50 mM MES and 2% NaCl (Carl Roth) in dH_20) and finally with Buffer 1. The samples were resuspended in 1 mL of Digestion buffer (pH 8, 20 mM Tris-HCl (Carl Roth) and 0.5% SDS in dH_20) to which 10 μL of 2 mg/mL proteinase K (Ambion) was added. The samples were incubated for 4 h at 50°C with shaking at 1400 rpm. After washing with Buffer 3, and three times with dH_20, the samples were resuspended in 1 mL of 0.1 M NaOH (Carl Roth) and incubated for ~16 h at RT with shaking at 1400 rpm. Afterward, the samples were centrifuged for 1 min at 16 000 x g, from which the supernatant, containing the wall teichoic acids was taken off and transferred to a new tube. The pH was neutralized by the addition of 250 μL of 1 M Tris-HCl. The isolated wall teichoic acids were analyzed by running the preheated samples on a 16% NuPage Tricine gel (Invitrogen) for 90 min at 125 V. The gel was stained with the Pierce silver stain for mass spectrometry kit (24600, Thermo Fisher Scientific), following the manufactures instructions. Briefly, the gel was first washed twice in dH_20, fixed in a solution of 30% ethanol (Sigma-Aldrich):10% acetic acid (glacial, Merck). The gel was further washed twice in 10% ethanol and twice in dH_20. Subsequently, the gel was sensitized for 1 min, washed twice with dH_20 and stained for 30 min. The gel was developed and a 5% acetic acid solution was added to stop the development. Images were recorded with the Molecular imager GelDoc XR+ (Bio-Rad).

QUANTIFICATION AND STATISTICAL ANALYSIS

All statistical analyses were done using GraphPad Prism v9.01 software and the R statistical environment. Statistical differences were determined using indicated methods with statistical significance set at a p-value ≤ 0.05 shown as one asterisk *, $p \leq 0.01$ as **, $p \leq 0.001$ as *** and $p \leq 0.0001$ as ****. All statistical details of experiments can be found in the figure legends.